Optimizing The Variability In The Deformation Of A Biomimetic Pinna

Abdulrahman Alenezi

Dissertation submitted to the faculty of the

Virginia Polytechnic Institute and State University

in partial fulfillment of the requirements for the degree of

Ph.D

In

Mechanical Engineering

Rolf Mueller, Chair

Alexander Leonessa

Michael Bartlett

Marco Corradi

January 23, 2023

Blacksburg, Virginia

Keywords: Pinna, biomimetic, and biosonar

Optimizing The Variability In The Deformation Of A Biomimetic Pinna

Abdulrahman Alenezi

Abstract

Bats are noted for having extremely powerful biosonar systems that enable them to move through and hunt through the thick foliage. They have a single emitter (mouth or nose) and two receivers in their biosonar system (ears). Some bat species, such as those belonging to the group's rhinophid and hipposiderid, feature intricate pinna motion patterns. These pinnae are divided into two groups: stiff movements and non-rigid motions. To understand how pinna sense worked has been studied in this thesis. The rigid pinna movements displayed a significantly different rotation, with revolutions axes spanning 180° in horizontal and curvature, according to axis-angle representations. The classification of landmarks on the pinna surface has explained two types of non-stiffed pinna movements. Additionally, a bio-inspired pinna has been used to explore the acoustic impact of the stiff pinna movements. All the given results showed precise accuracy in the motion of variance bats pinnae.

The research initiative was initiated with a comprehensive exploration of various design concepts, primarily focused on elucidating the intricate interplay between actuator geometry and the resultant deformation of the pinna. Employing a structured design code facilitated the generation of an array of configurations, each subject to stringent conditions and parameter settings necessitating subsequent validation.

After this design exploration, a tri-tiered hierarchy of forces, encompassing nominal, intermediate, and elevated magnitudes, was applied to instigate a systematic optimization process aimed at determining the most favorable deformation pattern. Computational simulations leveraging Finite Element Analysis (FEA) were conducted, accompanied by a rigorous material characterization procedure, to effectively quantify the extent of deformation across the array of configurations.

A consequential phase of the investigation involved the implementation of Principal Component Analysis (PCA) to differentiate the inherent variability within the different deformation arrangements, shedding light on their relative structural and morphological distinctions.

The culmination of the study encompassed the utilization of the Genetic Algorithm (GA), a sophisticated optimization technique, to facilitate the fine-tuning of deformation patterns in pursuit of the overarching goal: the deliberate induction of substantial and diverse variations in pinna morphology.

In summary, the research trajectory progressed sequentially through design conceptualization, force-induced optimization, computational simulations incorporating FEA and material characterization, Variability analysis via PCA, and culminated in the deployment of the GA to achieve the prime objective of inducing pronounced variability in pinna configuration.

The work was done as following, starting with design concepts, the main benefit of this is to understand how the geometry of actuator affects the pinna deformation. Using the design code to present several configurations that must have conditions and parameters to be validated. After that applying 3 different forces (zero, medium, and high) to get

the optimization for pattern. Applying the FEA simulations with help of material characterization to display the displacement of the arrangements. Finally doing the Variability analysis by using the principal component analysis. Then concluding the work by using the Genetic algorithm for optimizations to reach the main goal which is large variability in the pinna shape.

Optimizing The Variability In The Deformation Of A Biomimetic Pinna

Abdulrahman Alenezi

General Audience Abstract

This research delves into the fascinating world of bats and their extraordinary biosonar systems, specifically focusing on the intricate mechanics of their pinnae—the external ear structures. Bats, known for their remarkable ability to navigate dense foliage using biosonar, have been a subject of keen scientific interest. The study explores the design and functionality of bat pinnae, with a special emphasis on understanding how different movements contribute to their biosonar capabilities.

The investigation began with a comprehensive exploration of design concepts, aiming to unravel the complex relationship between actuator geometry and pinna deformation. A structured design code was employed to generate a range of configurations, each subjected to stringent conditions and parameters, requiring subsequent validation.

Following this design exploration, a three-tiered hierarchy of forces—ranging from nominal to elevated magnitudes—was applied to initiate a systematic optimization process. Computational simulations, utilizing Finite Element Analysis (FEA) and rigorous material characterization, were conducted to quantify the extent of pinna deformation across various configurations.

The study further implemented Principal Component Analysis (PCA) to discern inherent variability in different deformation patterns, shedding light on their structural and morphological distinctions. The research culminated in the deployment of the Genetic Algorithm (GA), a sophisticated optimization technique, to deliberately induce substantial and diverse variations in pinna morphology.

In summary, the research trajectory progressed from design conceptualization to force-induced optimization, incorporating computational simulations and material characterization. Variability analysis through PCA provided insights into structural distinctions, and the use of the Genetic Algorithm aimed at achieving the overarching goal of inducing pronounced variability in pinna configuration. This work not only enhances our understanding of bat biosonar systems but also offers potential applications in bio-inspired design and acoustic engineering.

Acknowledgements

I would not be able to be here today without the help of Prof. Mueller. I need to say he makes the time to see me more than 5 times a day. I have had lots of obstacles and problems but thanks God that he is there always takes my hand and support me and guide me.

Prof. Leonessa, Prof. Bartlett, Prof.Corradi, my mother, My Family, My brothers, Mubark Alrmudi ,Abdullah Alqahtani Arwa, Boja for his helped in design space, and My friends. A special thanks to Dr. Ahmed Husain, Dr, Chris Fuller, Dr. Saad and Dr.Saied Taheri.

A special thanks to Dr. Mohammed, Dr. Muneiah for all the support.

I would like to thank my brothers. I will not be able to do it without the help of Dr.Aimee, and Cathy. Thay are the hidden soldiers.

Thank you all.

Table of Contents

List of Figures

List of Tables

Declaration

I declare that the work contained in this thesis has not been submitted for any other award and that is all my own work. I also confirm that this work fully acknowledges opinions, ideas, and contributions from the work of others.

I declare that the Word Count of this Thesis, excluding bibliography and appendices, is 20205 words.

Name: Abdulrahman Alenezi

Signature:

Date: 01/23/2024

Chapter 1 Introduction

1.1 Research background

The outer ear, or pinna, of animals has evolved over millions of years to perform a variety of functions, including sound localization and sound amplification (Nothwang, 2016). Scientists and engineers have been studying the pinna's design to create biomimetic devices that can replicate its functionalities (Chen Austin et al., 2020). One area of interest is optimizing the variability in the deformation of a biomimetic pinna (Yin & Müller, 2021).

To understand why optimizing variability in the deformation of a biomimetic pinna is important, it is necessary to first understand the structure and function of the pinna (Sutlive et al., 2020). The pinna is composed of a cartilaginous framework covered by skin (Bhandari, 1998). The shape and size of the pinna vary across species, and within species, it can vary based on factors such as age, gender, and genetics (Okoro et al., 2012). The pinna is responsible for collecting and amplifying sound waves, which then travel through the ear canal to the eardrum (Sundar et al., 2021).

The pinna's shape plays a critical role in sound localization (Chiang-Jung Pu et al., 1997). The sound waves that enter the ear canal are influenced by the shape and orientation of the pinna (Rabbitt & Holmes, 1988). The pinna acts as a sound filter, altering the frequency content of the incoming sound waves based on the shape of the ear (Rice et al., 1992). The changes in frequency content provide important information

about the location of the sound source. This information is then used by the brain to determine the direction of the sound.

In addition to its role in sound localization, the pinna also plays a role in sound amplification. The shape of the pinna can act as a resonator, amplifying certain frequencies of sound waves (Bailey, 1993). This can be particularly useful for animals that need to detect low-frequency sounds, such as elephants or whales.

Scientists and engineers have been studying the pinna's design to create biomimetic devices that can mimic its functionalities (Bar-Cohen, 2011). One approach is to create a synthetic pinna that can replicate the shape and deformation characteristics of the biological pinna. By doing so, researchers hope to create devices that can improve sound localization and amplification in a variety of applications, from hearing aids to robots.

However, creating a synthetic pinna that can replicate the variability in the deformation of the biological pinna is a challenging task. The deformation of the pinna is influenced by a variety of factors, including the direction and frequency of the incoming sound waves, the shape and size of the ear, and the properties of the skin and cartilage (Jung et al., 2019). Optimizing the variability in the deformation of a biomimetic pinna requires a deep understanding of the underlying mechanics of the pinna and the ability to replicate these mechanics in a synthetic structure (Liu et al., 2020).

To address these challenges, researchers have been exploring a variety of approaches, including the use of advanced materials, such as shape-memory polymers, and the use of computational models to simulate the deformation of the pinna. By combining these

approaches, researchers hope to create biomimetic devices that can replicate the variability in the deformation of the biological pinna.

The development of biomimetic devices that can replicate the functionalities of the pinna has broad implications for a variety of fields, from audiology to robotics (Argentieri et al., 2013). For example, hearing aids that can replicate the functionalities of the pinna could provide improved sound localization and amplification for individuals with hearing impairments. Similarly, robots that can replicate the functionalities of the pinna could be used in applications such as search and rescue, where the ability to detect and locate sound sources could be critical.

In this regard, optimizing the variability in the deformation of a biomimetic pinna is an important area of research that has the potential to improve sound localization and amplification in a variety of applications. Optimizing the variability in the deformation of biomimetic pinnae could lead to more accurate and reliable artificial hearing systems. By mimicking the natural capabilities of the pinna, these systems could improve sound localization accuracy in a range of applications, from hearing aids to robotics. However, this is a challenging task that requires a deep understanding of the underlying mechanics of the pinna and the ability to replicate these mechanics in a synthetic structure. The development of biomimetic devices that can replicate the functionalities of the pinna.

Therefore, this study investigates the understanding of how the pinna senses work. It explores the rigid movements of the pinna, which exhibit a distinct rotation with revolution axes spanning 180° in both horizontal and curvature dimensions, as represented by axis-angle representations. The study also identifies two types of non-stiffened movements based on landmark classification on the pinna surface.

1.2 Research aims and objectives

The aim of this thesis is to investigate and develop approaches for optimizing the variability in the deformation of a biomimetic pinna. This involves understanding the underlying mechanics of the pinna and its role in sound localization and amplification, exploring advanced materials and computational models for replicating the pinna's deformation characteristics, and evaluating the performance of biomimetic devices in sound localization and amplification tasks. The goal of this research is to contribute to the development of improved biomimetic devices for sound localization and amplification, with potential applications in fields such as audiology, robotics, and engineering.

i. Generate design space for the pinna and actuators with different configurations of the controlled 4 parameters: location (x,y), orientation, and length.

ii. Generate a valid FEA numerical model for the pinna and actuators to define the fitness function to evaluate the solution domain.

iii. Perform variability analysis of the pinna deformations that can be achieved with different actuator configurations using standard methods of PCA.

iv. Optimizing the actuators configuration based on the design space, numerical simulation, and variability quantification, using Genetic Algorithms.

1.3 Contribution to knowledge

This research endeavors to make significant contributions to the field of auditory perception, sound localization, and the understanding of non-rigid pinna motions. By addressing the limitations identified in previous studies, the following contributions are anticipated:

1.3.1 Enhanced understanding of non-rigid pinna variability:

By expanding the dataset of non-rigid pinna motion sequences, this research is providing a more comprehensive exploration of the variability in these motions. The increased sample size will enable a more accurate characterization of the diverse range of non-rigid pinna movements, leading to a refined understanding of their implications for auditory perception.

1.3.2 Practical applications in auditory research:

The findings of this study have the potential to be directly applied in various auditory-related applications. Knowledge about non-rigid pinna motions and their variability can inform the development of improved sound localization algorithms, hearing aid designs, and virtual auditory environments, enhancing the overall auditory experience.

1.3.3 Design configuration:

This research providing a novel Algorithm for Actuator Placement: Developing a novel algorithm or method for placing five actuators on the pinna while ensuring they do not overlap and are fully placed. This could involve innovative geometric constraints or optimization techniques.

Biomimetic Design: Incorporating biomimetic principles into the actuator placement, mimicking natural pinna structures, which can lead to unique and innovative solutions.

1.3.4 Comprehensive non-rigid pinna characterization through FEA:

Customized Deformation Prediction: Creating custom simulation scripts (parametric study) for predicting pinna deformations based on actuator configurations and activation levels. This customization can lead to more accurate and efficient simulations tailored to your specific application.

Integration with Standard Software: Adapting and scripting standard software (e.g., Ansys) to predict deformations based on actuator configurations, providing a robust and reliable platform for analysis.

1.3.5 Dimensionality reduction and visualization using PCA:

Multifaceted Characterization: Using a combination of traditional statistical techniques (e.g., PCA) to characterize the variability in deformations. This integration of different approaches can reveal unique insights and patterns in the data.

Pinna-Specific Variability: Focusing on the variability in pinna deformations, which may be different from generic approaches and can lead to specialized insights for your application.

1.3.6 Optimized subgroup differentiation with genetic algorithms:

This research using genetic Algorithm Exploration: Investigating genetic algorithms for optimizing actuator configurations in the context of pinna deformations. This approach is innovative and can efficiently search the design space for configurations that maximize variability.

Feedback-Driven Optimization: Incorporating feedback from the variability analysis step to guide the optimization process, allowing for a dynamic and adaptive approach to actuator configuration discovery.

1.3.7 Enhanced understanding of auditory perception:

The combined application of FEA, PCA, and GA will lead to a deeper understanding of how non-rigid pinna motions influence auditory perception and sound localization. By unraveling the complex relationship between biomechanics and auditory processing,

this research will provide insights into the mechanisms underlying human acoustic experiences.

1.3.8 Innovative methodological framework:

This research introduces an innovative framework that combines biomechanical simulations, dimensionality reduction, and optimization techniques. The integration of FEA, PCA, and GA can serve as a blueprint for studying other complex systems with high-dimensional data, broadening the methodological toolkit available to researchers.

1.4 Thesis structure

The Thesis organization is as follows:

- Chapter 1 provides an introductory overview of the subject focused on optimizing variability in the deformation of a biomimetic pinna. Additionally, explicitly outlines the objectives, aims, and contributions to knowledge.
- Chapter 2 presents the literature review concerning biomimetic pinnae and their optimization for variable deformations, which falls within the scope of this research.
- Chapter 3 illustrates the research methodology embraced in this thesis, commencing with the design concepts, followed by the exploration of the design space. Subsequently, it involves the utilization of finite element analysis tools for numerical simulations, followed by the application of principal component

analysis to assess variability. Finally, it incorporates the utilization of genetic algorithms for the purpose of optimization.

- Chapter 4 highlights the design space, articulates the conceptualization of pinna actuators, visualizes the array of actuator configurations within the design space, and culminates with an exploration of the activation patterns of these actuators.
- Chapter 5 shows the numerical predictions of pinna deformations, considering a specified actuator configuration and activation levels (none, medium, high). The deformation predictions will be generated through a standard software platform (such as Ansys) that is customized to accommodate the provided actuator configuration.
- Chapter 6 the range of deformations attainable through various actuator configurations will be assessed using the standard methodology of Principal Component Analysis (PCA).
- Chapter 7 utilizing the design space, numerical simulations, and quantified variability, the objective is to identify and apply an optimization approach that can uncover an actuator configuration capable of generating significant variability in pinna deformations. Genetic algorithms will be explored as potential tools for achieving this goal.
- Chapter 8 The harmonic acoustic model, applied to pinna testing, uncovers how the outer ear responds to different frequencies. It highlights the pinna's frequency response, revealing how its shape influences tone filtering and resonance. This model aids in understanding the pinna's role in sound localization by identifying resonance frequencies crucial for spatial perception.

Alongside computational models rooted in the harmonic acoustic framework predict the interaction between sound waves and the pinna, offering a theoretical basis for experimental design and interpretation of the pinna's complex acoustic properties.

- Chapter 9 this section provides a condensed overview of the principal discoveries, offers the primary conclusions drawn from the study, and puts forth suggestions for prospective research endeavors.

Chapter 2 Literature review

2.1 Review of biomimetic pinna

Biomimetics researchers have been studying the pinna's design to create synthetic structures that can replicate its functionalities (Corni et al., 2012). One approach is to create a synthetic pinna that can replicate the shape and deformation characteristics of the biological pinna (Bhamare et al., 2022). By doing so, researchers hope to create devices that can improve sound localization and amplification in a variety of applications, from hearing aids to robots (Heidemann et al., 2006).

Designing an artificial outer ear, also known as a pinna, that can accurately mimic the complex deformations of a real biological pinna poses a significant challenge (Schillebeeckx et al., 2011). The deformation of the pinna is affected by various factors, such as the angle and frequency of incoming sound waves, the size and shape of the ear, and the properties of the skin and cartilage (Wang et al., 2021). Achieving optimal variability in the deformation of a synthetic pinna that imitates nature requires a comprehensive understanding of the underlying mechanics of the biological pinna and the capacity to reproduce these mechanics in an artificial structure (Ren et al., 2019).

Researchers have been exploring a variety of approaches to address these challenges. One approach is the use of advanced materials, such as shape-memory polymers, that can mimic the deformation characteristics of the biological pinna (Apsite et al., 2022). These materials can be programmed to respond to specific stimuli, such as temperature or light, to mimic the deformation of the pinna. Another approach is the use of

computational models to simulate the deformation of the pinna (Buytaert et al., 2011). These models can be used to optimize the design of biomimetic devices and evaluate their performance in sound localization and amplification tasks.

The development of biomimetic devices that can replicate the functionalities of the pinna has broad implications for a variety of fields, from audiology to robotics (Argentieri et al., 2013, 2015). For example, hearing aids that can replicate the functionalities of the pinna could provide improved sound localization and amplification for individuals with hearing impairments. Similarly, robots that can replicate the functionalities of the pinna could be used in applications such as search and rescue, where the ability to detect and locate sound sources could be critical.

2.2 Review on optimizing the variability in the deformation of a biomimetic pinna

Biomimetic pinna is an emerging technology that seeks to replicate the functionalities of the biological pinna (Peremans & Reijniers, 2005). One key challenge in creating a biomimetic pinna is optimizing the variability in its deformation. Several researchers have explored different approaches to address this challenge.

One approach is the use of advanced materials that can mimic the deformation characteristics of the biological pinna (Burdick & Prestwich, 2011). Shape-memory polymers are one such material that can be programmed to respond to specific stimuli, such as temperature or light, to mimic the deformation of the pinna (Apsite et al., 2022). Another approach is to create a flexible structure that can deform in response to the direction and frequency of the incoming sound waves (Lee et al., 2014). This approach

involves creating a synthetic structure that can replicate the shape and deformation characteristics of the biological pinna, such as the curvature of the concha and the shape of the helix (Chung et al., 2018).

Computational modeling is also an important tool for optimizing the variability in the deformation of a biomimetic pinna (Müller et al., 2012). Finite element analysis (FEA) is a common approach for simulating the deformation of the pinna (Serafin et al., 2018). FEA involves breaking down the pinna into small elements and modeling their deformation in response to different stimuli. This approach can provide insights into the underlying mechanics of the pinna and inform the design of biomimetic devices (Müller et al., 2018).

Another key consideration in creating a biomimetic pinna is the selection of appropriate materials. The materials used should have mechanical properties that are similar to those of the biological pinna, such as the Young's modulus and Poisson's ratio (Shao et al., 2012). Silicone rubber and polyurethane have been identified as promising materials for biomimetic pinna applications (Li et al., 2018).

The applications of biomimetic pinna technology are broad. One potential application is in the development of hearing aids that can replicate the functionalities of the pinna (Schillebeeckx et al., 2011). These hearing aids could provide improved sound localization and amplification for individuals with hearing impairments (Byrne & Noble, 1998). Biomimetic pinna technology also has applications in robotics. Robots that can replicate the functionalities of the pinna could be used for sound source

localization and tracking tasks, as well as for improving speech recognition in noisy environments (Kim & Okuno, 2013).

Several studies have been conducted to optimize the variability in the deformation of a biomimetic pinna. One approach is the use of advanced materials, such as shape-memory polymers, that can mimic the deformation characteristics of the biological pinna (Apsite et al., 2022). These materials can be programmed to respond to specific stimuli, such as temperature or light, to mimic the deformation of the pinna. Another approach is the use of computational models to simulate the deformation of the pinna, which can be used to optimize the design of biomimetic devices and evaluate their performance in sound localization and amplification tasks (Müller & Kuc, 2007).

Fu et al. (2021) demonstrated the potential of shape-memory polymers in creating biomimetic pinna devices. They developed a biomimetic pinna made of a shape-memory polymer that was able to change its shape in response to temperature changes. The device was able to mimic the deformation characteristics of the biological pinna and showed promising results in sound localization and amplification tasks.

Different researchers worked on the motion of bat pinna to find the variability in the motion of bat pinna. (Fujioka et al., 2021) studied different species of bats that can transmit sound waves in all three-dimensional (3D) space. The article discussed the impressive eyesight and sensing abilities of bats. Bats have two types of watching abilities: spatial resolution and temporal resolution, which make it easy for them to locate things efficiently. Bats were also observed to have great sensing power, with two transmitters and one receiver that allowed them to sense things even at night. This ability is unique to bats and cannot be replicated by the latest technology tools. This ability is remarkable considering the advancements made by humans, including

reaching the moon. However, humans can still benefit from bats' abilities, including their eyesight and listening sense (Teshima et al., 2022). Bats also had the ability to sense common habits by changing their heartbeats, which is impressive to listen to. They can listen to sound in 3D space and gather information from their two receivers to find variability, which is useful for bio-inspired robot ear motion. The article highlights the remarkable abilities of bats and the potential benefits for humans to learn from and utilize these abilities in technology and other fields.

(Pulver et al., 2022) investigate the animals that were killed and disturbed at the beginning of the universe. They discussed the competition between hunters and prey and the impact it has had on animal populations, with many animals losing their lives or their hearing sense. Insects were noted for their ability to hear using pairs of receivers, which allowed them to sense things that humans cannot. Their ears had a wide range of frequency equipment, which made them very effective. Other animal species also had similar abilities gifted by nature. The article goes on to describe how the abilities of bats and other animals have been studied using simulation software, which involved designing a 3D geometry of the ear using computational fluid dynamics and performing meshing using finite element analysis. This research focused on bat-ear motion and bio-inspired robot ear motion to find variability, which could be useful for developing new technologies. Overall, the article highlights the impressive hearing abilities of insects and other animals and the potential benefits of studying and learning from their natural abilities to develop new technologies.

Zalapa et al. (2022) investigated that bats have ears outside of their body which helps them to sense the things outside the environment. They focused on the importance of outside ears for bats to listen to various sound waves. If a bat is injured in this part of its

body, it can reduce its ability to sense sound wave reflections. Some bat species, such as Saba's short-tail and ghost bats, are prone to dangerous inherited illnesses that can affect their hearing ability. These illnesses include pinna tumors, which can cause crusting, swelling, redness, and tissue damage. These bat species are found in various countries, including South Africa, Malaysia, and New Zealand. They noted that New Zealand has a relatively small number of bats with injuries and no hearing loss, while India has flying bat species. The study of bat-ear motion and bio-inspired robot ear motion can help find variability and potentially aid in developing new technologies. The article highlights the importance of the outside ears of bats for their hearing abilities and the potential consequences of inherited illnesses on their ability to sense sound waves.

(Hiraga et al., 2022) investigated the electrical waves generated by the bats by using their ears and noses respectively, sound waves are transmitted to the atmosphere and the bats receive back the reflections of those sound waves which were transmitted with the help of their ears which senses the three-dimensional surroundings. They described the complex mechanism by which bats used their ears to detect and locate prey in complete darkness. Bats had the ability to rapidly move their ears, which allowed them to accurately locate prey based on the sound waves reflected from their environment. They discussed how that bat-ear motion can be translated into bio-inspired robot ear motion, which could potentially improve the accuracy and efficiency of sound localization in robotic systems. The article highlights how the design of the robot ear can be informed by the structure and function of the bat ear. This involves analyzing the shape and movement of the various ear structures, such as the outer ear, the ear canal, and the eardrum, and developing artificial structures that can mimic these features. They demonstrated the potential of using bio-inspired design principles to improve the

performance of robotic systems, particularly in areas where animals had evolved unique sensory abilities. The use of bat-inspired ear motion could be especially useful in applications such as search and rescue missions, where robots must locate and rescue victims in challenging environments.

Another study by (Sutlive et al., 2020) designed a biomimetic pinna with an adjustable curvature that can be controlled using piezoelectric actuators. The device was shown to significantly improve sound localization compared to a conventional hearing aid. Similarly, a study by Xu et al. (2021) developed a biomimetic pinna-inspired acoustic sensor for sound source localization in a noisy environment. The device was shown to have a higher accuracy in sound source localization compared to conventional sensors.

The development of biomimetic devices that can replicate the functionalities of the pinna has broad implications for a variety of fields, from audiology to robotics (Argentieri et al., 2013). For example, hearing aids that can replicate the functionalities of the pinna could provide improved sound localization and amplification for individuals with hearing impairments. Similarly, robots that can replicate the functionalities of the pinna could be used in applications such as search and rescue or surveillance.

Many kinds of bat species exist in this world having many attributes in them. The bat's pinnae can sense their prey target one million times more than a human (Müller, 2015). They have millions of sense organs in their body that can sense every condition whether it's a day or night or in any season. In the world, there are more than 1200 bat species that have the ability in them to sense and find the location of any object, and most importantly they can find and classify their targets very easily with the help of their organs. They also have a biosonar system in their organs which helps the bats to sense

any kind of object (Boonman et al., 2014). They utilized their biosonar system for the detection of their targets for getting something to eat. This unbelievable ability of the bat pinna can be described as when the ultrasonic echoes which work as the single independent variable are received by the bat pinna species. They used different kinds of echoes from the natural environment and utilized them with the help of a biosonar system for the detection of any object or any prey target.

There are two levels through which the bat pinna can sense different kinds of objects. The basic example of the first level of bat pinna is the time-frequency basics which are different with different stages (Zhang & Mueller, 2022). These kinds of structures are found in the ultrasonic pulses of the bat. However, the biosonar system in the different species of bat pinna is frequency-modulated (FM) during their whole process of sensing. While other species of bat pinna have different types of frequency such as constant frequency (CF) section. Some of these bat species are called old world-leaf-nosed bats, these kinds of species are like a family species. The constant frequency (CF) section in the bat pinna is used to describe the doppler shifts. The Doppler shift is the process which is produced by the Federation of targeting different types of insects and it also can be compared with the other prey targets which are detected by the new type of species of bat pinna. Whereas the frequency-modulated component helps the bat to get the correct range of the target and it also explains to the bat the different kinds of properties of the target.

Since there are many kinds of bats in the whole world but some of these types have a special ability to sense any object in any situation. They have a biosonar system in their body as well as special types are organs that help the bats for detecting their prey targets and any other object (Fenton et al., 2014). Hipposiderids and rhinolophids are the two

types of bats that could exit the pulses of the biosonar system by their nostrils (Pedersen & Müller, 2013). The nostrils are part of the bat. When the bat emits the pulses, it also leaves the nose. The nose leaves a section of the bats that is very important for the emission of pulses of the biosonar system. The two types of bats named hipposiderid and rhinolophid bats have pinnae (ears) in their body that can be defined by their geometric features. These geometric features consist of antitragus and horizontal bridges as well.

2.3 Concluding remarks

In this study, the explanation of the different species of bat pinna and sensing organs with biosonar system is discussed. The pinna motions are generated when the bat emits the pulses of the biosonar system and these emissions of biosonar pulses can affect the echoes that are returned from the pinna to the environment. The pinna functions activate when they receive sound waves from the natural environment and the motion depends on the signal of the biosonar system as well. The pinna motions are very crucial for the detecting system of the bats by changing the geometry of the received sound signals. This helps the bats to sense their prey target or any other object. These changing sound waves of the biosonar system increase the efficiency of the bats and degrees of freedom which helps the bats to find their target after receiving these signals. By using the whole system, the bats detect their prey targets, and it is only an ability that occurs in bats. Many experts are trying to design this kind of extraordinary system so that humans can also take advantage of this wonderful system.

2.4 State of art

The research landscape in biomimetic design is rich and diverse, as reflected in the summary table. Actuator geometry and morphology are central themes explored by various authors, each focusing on different organisms or structures. Apsite et al. (2022) delve into smart soft design with a bioinspired approach, utilizing shape memory polymers for robotic applications. In contrast, Chung et al. (2018) concentrate on the curvature of concha and helix profiles, employing 3D bioprinting techniques for customized implants. Wang et al. (2021) explore the computational aspects of the human ear for phonetics, emphasizing user authentication. Li et al. (2018) venture into human skin layers, utilizing microcellular polyurethane foam and machine learning for high-performance skin morphology with temperature and electrochemical controls. The aquatic realm inspires Fu et al. (2021) in creating soft tiny swimmers using shape memory polymers for sound localization and amplification. The study by Fujioka et al. (2021) focuses on bats, analyzing collective behavior through high-sensitivity stereo camera recording and echolocation via ultrasound emissions. Pulver et al. (2022) contribute insights into bat biomimicry, investigating 3D ear geometries for large sound pressure gains and ultrasonic audiograms for enhanced detection. Hiraga et al. (2022) delve into bat morphology with active listening and mathematical modeling, aiming to design active sensing devices. Sutlive et al. (2020) explore pneumatic type actuators with eight variations for

adaptive sensing in autonomous system design inspired by bats. Bhamare et al. (2022) employ tissue engineering methods for human ears, conducting electron microscopy analysis for optimized clinical medical object design. Finally, Alenezi & Müller (2024) optimize actuator concepts using spatial distribution and 2D design space representations for bat-inspired structures, employing FEA, machine learning, and genetic algorithms to optimize deformation variability and enhance acoustic performance. This comprehensive overview highlights the diverse strategies employed in biomimetic design and their varied impacts across different application domains as shown in table 1.

Table 1: State of art.

Author	Design Parameters				Morphology				Impact
	Actuator (Size &Shape)	**Actuator (Position &Angle)**	**Design Focus**	**Pinna Material**	**Stiff Movement Characterisation**	**Non-Rigid Motion Characterisation**	**Deformation Variability Analysis**	**Large Variability Optimisation**	
Wang et al, 2021	No	No	Human Ear	No	Computational Techniques (Phonetics)	No	Acoustic Sensing Approach	No	User Authentication
Apsite et al, 2022	Smart Soft	Smart Soft	Bioinspired Design (General)	Shape Memory Various Polymers	No	No	Natural Stimuli	No	Robotic Applications (General)
Chung et al, 2018	No	No	Curvature of Concha and Helix Profiles	Auricular Cartlidge	No	No	No	3D Bioprinting Techniques	Customised Implants
Li et al, 2018	No	No	Human Skin Layer	Microcellular Polyurethane Foam	No	No	Machine Learning using Principle Component Analysis	Tempreture and Electochemical Controls	High Performance Skin Morphology
Fu et al, 2021	Biomimetic Inspired Aquatic	Biomimetic Inspired Aquetic	Soft Tiny Swimmers (Robotics)	Shape Memory Polymers	Thrust	Spiral	Theoretical	No	Sound Localisation and Amplification

Fujioka et al, 2021	No	No	Bat	No	No	3D Flight Path Analysis	No	Collective Behaviour Analysis Using High Sensitivity Stereo Camera Recording	Echolocation using Ultrasound Emissions
Pulver et al, 2022	Bioinspired	Bioinspired	Bat	No	Biophysic of 3D Ear Geometres using CFD FEA Techniques	No	No	Large Sound Pressure Gains Analysis	Ultrasonic Adiograms for Enhanced Detection
Hiraga et al, 2022	No	Natural Elevation Angles and 3 Axis Rotation	Bat	No	Active Listening and Mathematical Modeling	Pseudo Movement Modeling	Theoretical	No	Designing Active Sensing Devices
Sutlive et al, 2020	Pneumatic Type	8 variations	Bat	No	8 motions using Fill and Release Mechanisms	No	Stereo Vision Analysis (Non Linear)	No	Adaptive Sensing in Autonomous System Design
Bhamare et al, 2022	No	No	Human Ear	Tissue Engineering Methods	No	No	Electron Microscopy Analysis	No	Optimised Clinical Medical Object Design
Alenezi & Müller, 2024	Optimisation of Actuator Concepts using Spacial Distribution, and Design Space 2D	180° Axis Angle Representations of Actuators Geometries	Bat	EcoFlex 50	Structural Analysis using FEA	Surface Landmark Analysis using FEA	Machine Learning using Principle Component Analysis	Population Selection using Genetic Algorithm	Optimizing the variability in the deformation of a biomimetic pinna to optimize acoustic performance

Chapter 3 Research methodology

3.1 Design concepts

The process of creating a concept design for the actuators involves a systematic exploration of various arrangements that can be attached to the back of the pinna, while adhering to specific criteria. The primary goal of this endeavor is to identify a suitable design that effectively addresses the requirements and constraints of the research.

The concept design phase begins by considering the unique anatomical characteristics of the pinna. The actuators need to be affixed to the pinna's rear surface in a manner that doesn't interfere with its natural shape or obstruct any functional features. To achieve this, the actuators are strategically positioned without overlapping.

One key aspect to address is the arrangement of the actuators. Each grouping of five actuators forms which is refered to as an "arrangement." These arrangements play a crucial role in determining the spatial distribution and impact of the actuators on the pinna. The design process involves experimenting with different configurations of these arrangements to achieve the desired effects.

In addition, the length and angle of each actuator within an arrangement are adjustable parameters. These parameters allow for a fine-tuning of the sound localization and auditory perception capabilities. By varying the lengths and angles, allows to create specific acoustic effects that align with the research’s objectives.

During this exploratory phase, computer-aided design (CAD) Fusion 360 software will be employed. This allows to visualize and analyze the impact of different arrangements, actuator lengths, and angles on the pinna deformaion. Iterative design cycles involve refining the arrangements. The main aim of Design concepts is finding Actuator design after going sevral tests.

3.2 Design space

Exploration of the design space is imperative to identify valid configurations for the pinna's actuators, involving the investigation of four parameters—location (x, y), orientation, and length—across five different actuators. The process entails adjusting the parameter ranges to discover a multitude of valid configurations, ensuring a thorough examination of the pinna's actuators. It is essential that the chosen parameters adhere to specific constraints for the configurations to be considered valid. To streamline this exploration and configuration generation process, a MATLAB code will be developed. This code will facilitate the randomization of parameters within the defined constraints, thereby enabling the efficient generation of diverse and valid configurations for the actuators, contributing to a comprehensive study of the pinna's mechanical behavior.

3.3 FEA numerical simulation

To comprehensively assess the deformation of the pinna resulting from the configurations derived through the exploration of the design space, an advanced computational approach in the form of Finite Element Analysis (FEA) simulations will be employed. FEA stands as a highly sophisticated and versatile tool, wielding computational prowess to predict and visually represent the intricate structural behavior and deformation patterns of complex geometries when subjected to a myriad of conditions. The FEA process intricately involves the subdivision of the pinna's geometric structure into a multitude of smaller elements, with each element meticulously representing a specific portion of the overall structure. These elements are interconnected at nodes, forming a dynamic network that enables the precise calculation of crucial parameters such as stress, strain, and deformation within the pinna. As the pinna is subjected to external forces and conditions, mirroring the effects exerted by the actuators aligned with the selected configurations, the FEA simulations facilitate an exhaustive understanding of how the pinna dynamically responds to these external influences. This comprehensive analysis, enabled by FEA, becomes instrumental in unraveling the nuanced mechanical intricacies and responses inherent in the pinna's structure, thus providing invaluable insights for further refinement and optimization in applications ranging from biomechanics to robotics.

3.4 Principle component analysis (PCA)

Principal Component Analysis (PCA) emerges as a pivotal technique within the intricate realm of bat pinna design, primarily harnessed for the purpose of dimensionality reduction. Operating as a fundamental tool, PCA proves invaluable in streamlining the overwhelming array of bat pinna parameters, concurrently bolstering comprehensibility while mitigating the risk of information loss. The core mechanics of PCA encompass a transformative process, wherein the myriad eigenvalues associated with bat pinna attributes are recalibrated into a condensed, lower-dimensional matrix of parameters. This strategic transformation not only expedites the analytical process but also cultivates a more nuanced understanding of variable variances inherent in the complex structure of bat pinnae. By navigating the multifaceted landscape of bat pinna parameters through PCA, designers and researchers can distill essential insights, fostering a deeper comprehension of the intricacies that define these biological structures. The application of PCA thus transcends mere dimensionality reduction, emerging as a powerful analytical lens that unveils hidden patterns and relationships within the expansive spectrum of bat pinna attributes.

3.5 Genetic algorithm (GA)

The genetic algorithm (GA), drawing inspiration from biological evolution, serves as a versatile methodology for optimizing challenges, whether constrained or unconstrained. In the specific context of bat pinna design, the GA systematically refines configurations through a series of key steps: population selection, crossover, mutation, and elitism. Initial potential solutions encompass a diverse range of pinna configurations, each evaluated for fitness based on the desired outcome. The selection process mirrors "survival of the fittest," with individuals chosen based on their fitness. Crossover combines genetic information, simulating recombination in natural evolution, while mutation introduces random changes, fostering diversity reminiscent of genetic mutations. Elitism preserves top-performing solutions, preventing regression. Iteratively applying these steps, the GA enhances fitness across generations until a predetermined stopping criterion is met. In the realm of bat pinna design, fitness scores are evaluated, with higher scores indicative of well-suited configurations. Maximum and average fitness values provide insights into the quality of solutions at different evolution stages. In essence, the genetic algorithm emulates natural selection, utilizing population selection, crossover, mutation, and elitism to iteratively evolve bat pinna configurations, ultimately enhancing their performance and effectiveness.

3.6 Acoustic analysis

Within ANSYS, the simulation of the bat's pinna acoustic behavior entails the intricate task of modeling both its complex geometry and material properties to scrutinize

interactions with sound waves. This software affords precise simulations of the pinna's shape, empowering researchers to delve into the influence it wields on the bat's echolocation prowess. ANSYS is equipped with advanced acoustics tools, allowing for the exploration of various facets such as frequency response, directional sensitivity, and resonance characteristics inherent to the pinna. Through these tools, researchers can extract invaluable insights into the intricate acoustic phenomena that underlie the bat's extraordinary auditory perception. ANSYS, with its capabilities, facilitates a comprehensive understanding of how the pinna's specific shape actively shapes sound reception, playing a crucial role in aiding the bat as it navigates its environment with exceptional acuity.

Chapter 4 Design space

4.1 Actuators geometry

The geometry of actuators plays a crucial role in determining the effectiveness and precision of pinna movement in various applications. The pinna, or the outer part of the ear, is involved in sound localization and can be manipulated by actuators for different purposes, such as in robotic systems, prosthetics, or virtual reality devices.

Here are some critical factors to consider in the design of actuators for pinna movement:

4.1.1 Actuator height and width

The dimensions of an actuator hold significant importance in determining its performance and interaction with the pinna. The width of the actuator directly influences the area it occupies on the pinna's surface, with a broader width resulting in a larger contact area. Meanwhile, the height of the actuator presents multifaceted implications. The base of the actuator governs the force required for movement initiation, with a larger base demanding greater force. The force head, responsible for applying force to the pinna, sees an increase in the gap between force heads when its size is amplified, leading to an escalation in deformation. The augmentation of force head dimensions contributes to a wider gap, accentuating deformation on the pinna. Striking a balance between the width and height is crucial for optimal performance,

precision in movement, and user comfort. Achieving this balance ensures that the actuator can replicate natural pinna movements accurately, making it well-suited for applications such as virtual reality or robotics. Overall, careful consideration of these dimensions is essential in designing actuators that effectively and comfortably interact with the pinna in various contexts.

4.1.2 Touch point

The touch point within the actuator design stands out as a pivotal factor with profound implications for its overall performance. The size of this touch point plays a decisive role in shaping the dynamics of force application on the pinna. A larger touch point tends to diffuse the applied force, spreading its impact over a broader area and diminishing localized pressure. Conversely, a smaller touch point concentrates the force, influencing shear force dynamics and creating a more focused sensation. Striking the right balance in choosing the size of the touch point is crucial for achieving precision in movement and managing user comfort. This consideration is particularly important in applications where the actuator comes into direct contact with the skin or sensitive areas. The optimal design must carefully navigate between effective force application and ensuring a positive and comfortable user experience. Furthermore, tailoring the touch point size to the specific requirements of the application, whether in virtual reality or robotics, ensures that the actuator performs optimally in diverse contexts.

4.1.3 Location of the actuators

The positioning of actuators is a pivotal element in achieving the desired outcome of pinna deformation. This outcome is intricately linked to the material's behavior, and a comprehensive understanding is obtained through rigorous tensile testing, particularly given its correlation with material thickness. The configuration of actuator geometry encompasses various considerations, including width, height, touch points, and precise positioning. Through a meticulous examination and accurate adjustment of these factors, an optimal design configuration can be defined. This tailored configuration is aimed at producing specific levels of pinna deformation, considering both biomechanical principles and the material properties involved. In essence, this holistic approach emphasizes the intricate interplay between design considerations and material characteristics, highlighting their collaborative role in achieving effective and controlled pinna deformation. The synthesis of these elements contributes to the development of actuators that can reliably and precisely replicate the intricate movements of the pinna in diverse applications.

4.2 Design concepts of pinna actuators

The actuator design process involved the creation of several concepts, but they were narrowed down to seven distinct concept designs. These designs exhibit a diverse range of shapes, including cylindrical, gear, trapezoidal, and cuboidal profiles, each incorporating 11 teeth. Notably, these designs go beyond conventional approaches, incorporating innovative adaptations to enhance functionality. Some of these adaptations include the integration of square holes, semi-cylindrical holes, and invert trapezoidal cutouts. Figure 1 outlined (a) shows cylindrical profile with 11 cylindrical teeth, (b) shows gear profile with 11 teeth, (c) shows Trapezoidal profile with 11 teeth, (d) shows cuboidal profile with 11 cylindrical teeth, (e) shows cuboidal profile with 11 cylindrical teeth, but each teeth has a square hole to make 2 pseudo teeth profile, (f) shows cuboidal profile with 11 cylindrical teeth, but each teeth has a semi-cylindrical hole profile, and (g) shows cuboidal profile with 11 cylindrical teeth, but each teeth has a cut out of invert trapezoidal.

These design variations aim to explore novel avenues for improving the actuator's performance and versatility, considering factors such as force distribution, precision, and overall efficiency. The inclusion of unique features underscores a creative and iterative approach in the pursuit of an optimal actuator design that aligns with specific application requirements. This comprehensive exploration of diverse concepts sets the stage for a thorough evaluation process to identify the most promising design for further development and implementation.

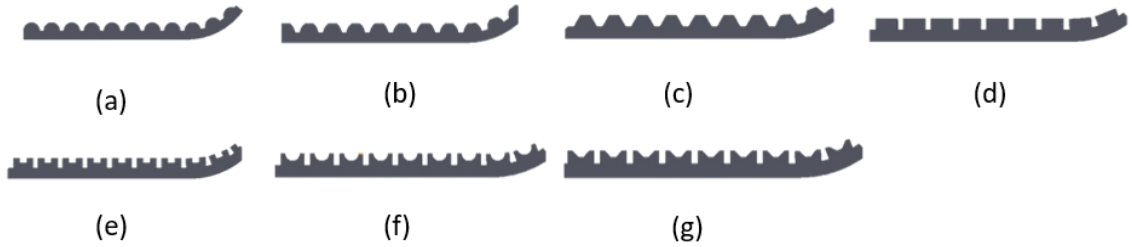

Figure 1: Design concepts of the actuators.

Table 2 provides a comprehensive overview of the load applied to all 7 actuators, serving as a crucial step in testing the boundaries of their geometry. This preliminary assessment is integral to understanding the individual capabilities and limitations of each actuator design. The load testing process serves as a valuable precursor to the subsequent phase, which involves advancing to the arrangement stage. In this subsequent step, the focus shifts towards the attachment of the actuator to the back of the pinna. The data obtained from the load testing phase will likely inform decisions about the optimal actuator design to be incorporated into the arrangement, ensuring that the collective system can effectively induce the desired pinna deformation. This systematic approach, moving from individual actuator testing to the broader context of arrangement, contributes to a thorough evaluation of the overall system's performance

and sets the groundwork for refining and optimizing the actuator configuration for practical applications.

Table 2: Summery of the load cases.

Case	Load Applied
Case 1	Surface contact load (0.000001 N)
Case 2	0.1N load at each actuator
Case 3	0.5N load at each actuator

Figure 2 presents the outcomes of the Finite Element Analysis (FEA) conducted on all seven concept designs of the actuators with the same naming and order were obtained from Figure 1. FEA is a powerful simulation method that allows for a detailed examination of the structural and mechanical behavior of the actuators under various conditions. The results of this analysis offer valuable insights into factors such as stress distribution, deformation, and overall structural integrity for each design. By employing FEA, the performance and robustness of the actuators can be systematically evaluated. This data is crucial in assessing how well each concept design withstands the applied loads, helping to identify potential weaknesses, areas of improvement, and opportunities for optimization. The FEA results are likely to guide the selection of the most promising actuator design or designs for further refinement and integration into the broader arrangement on the back of the pinna. This iterative process, combining real-world load testing with simulation-based FEA, contributes to the development of a robust and

effective actuator system capable of producing the desired pinna deformation with precision and reliability.

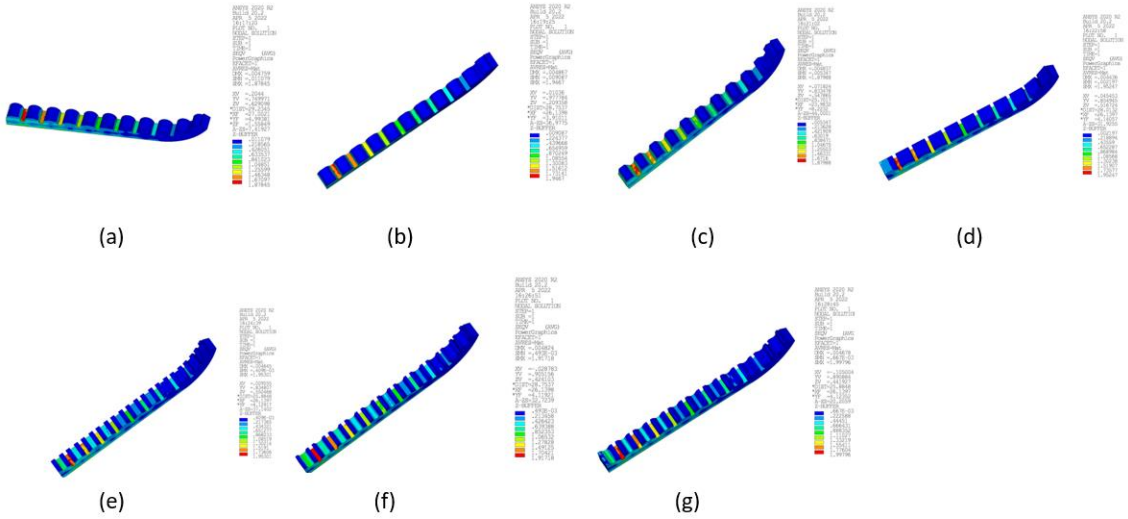

Figure 2 : FEA simulation results for all 7 concept designs of the actuators.

Based on the favorable outcomes observed in the evaluation of the 7 actuator design concepts, Concept 1 from Figure 1 emerges as particularly promising for the project's goals. Consequently, the logical progression involves advancing to the next testing stage, wherein Concept 1's characteristics will be further assessed for practical application. The subsequent phase includes attaching Concept 1 to the back of the pinna, transitioning from individual actuator testing to the arrangement phase. This evaluation encompasses not only Concept 1's stand-alone performance but also its collaborative effectiveness with other actuators in inducing the desired pinna deformation. This iterative approach ensures a systematic and informed development process, with the selected actuator design contributing seamlessly to the overall system functionality. The outcomes of integrated testing will guide refinements and

optimizations, ultimately leading to a reliable actuator configuration for the specified application. Furthermore, Figure 3 visually illustrates how an actuator can be affixed to the rear of the pinna. Despite focusing on a single actuator in the illustration, it's essential to note that a complete attachment involves using a total of 5 actuators, referred to as an "arrangement." The strategic placement of these 5 actuators is critical for achieving the desired pinna deformation and movement patterns. Figure 3 serves as a foundational reference for understanding the individual actuator's positioning within the broader context of the arrangement, contributing to a holistic understanding of the system's functionality.

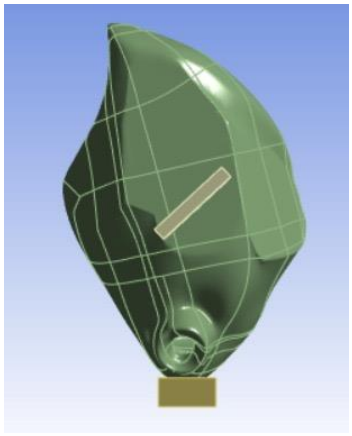

Figure 3: Actuator design 1 attached to the back of the pinna.

The choice of the first actuator for this investigation was guided by insights derived from previous results. This decision was particularly influenced by a focused consideration of tooth architecture, while keeping other parameters consistently controlled throughout the simulation of alternative actuators. The five designated positions (A, B, C, D, and E) were specifically chosen for analysis, and their visual representation can be found in the accompanying diagrams in Figure 4. Employing a strategic approach, this methodical exploration aims to understand how different

actuator positions, within the context of varied tooth architectures, impact stress distribution and, consequently, influence pinna deformation.

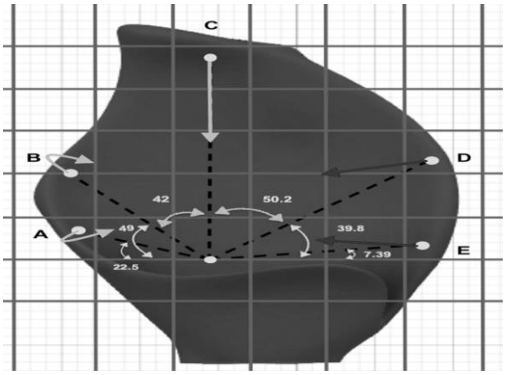

Figure 4: Positions of actuators on pinna (Arwa).

The simulation results have been consolidated and presented in Figure 5. Following a thorough examination of these results, Actuator Design 1, characterized by a cylindrical profile with 11 cylindrical teeth, has been chosen to progress into the subsequent stages of work on pinna deformation. This selection is based on the favorable outcomes observed in the simulation, indicating that Actuator Design 1 aligns well with the objectives of the study and exhibits promising characteristics for further exploration in the context of pinna deformation.

Pinna deformation	Actuator deformation figures				
	A	B	C	D	E
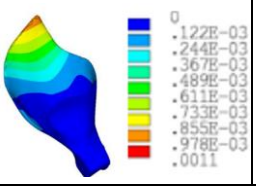				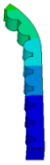	
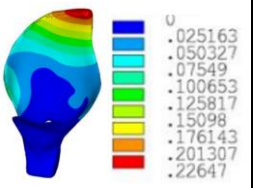		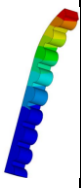	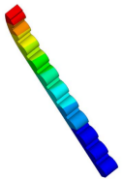		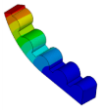
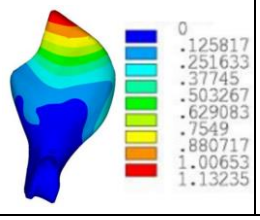	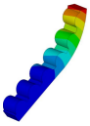		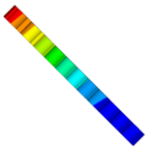		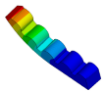

Figure 5: Summery of pinna deformation and actuators deflection.

Maximum stress and strain tests are commonly conducted on materials to assess their mechanical properties and performance under extreme conditions. These tests provide valuable information for engineers, researchers, and manufacturers in various industries. Here are some benefits of conducting maximum stress and strain tests:

Material Characterization:

Strength Assessment: These tests help determine the maximum stress a material can withstand before failure. This is crucial information for designing structures and components that need to withstand specific loads.

Elastic Modulus: The tests provide data on the material's stiffness or elastic modulus, which is essential for predicting how a material will deform under different loads.

Safety and Reliability:

Structural Design: Understanding the maximum stress and strain a material can endure is essential for designing structures with appropriate safety margins. This ensures that structures can withstand the expected loads without failure.

Product Durability: Manufacturers use these tests to evaluate the durability and reliability of products, ensuring they can withstand real-world conditions without unexpected failures.

Quality Control:

Material Quality: Maximum stress and strain tests are part of quality control processes in manufacturing. They help ensure that the materials used in a product meet specified standards and can handle the intended applications.

Failure Analysis:

Identifying Weaknesses: Conducting these tests allows researchers to identify weaknesses and failure modes in materials. This information is crucial for improving materials and designing more robust structures and products.

Optimizing Design:

Material Selection: Engineers can use the data from these tests to select the most appropriate materials for a given application. This helps optimize the design by choosing materials that offer the best balance of strength, weight, and cost.

Regulatory Compliance:

Industry Standards: Many industries have specific standards and regulations that dictate the minimum mechanical properties a material must possess. Conducting maximum stress and strain tests ensures compliance with these standards.

Research and Development:

Innovation: Researchers use these tests to explore new materials and design concepts. Understanding how materials behave under extreme conditions is crucial for pushing the boundaries of innovation in various fields.

Predicting Material Behavior:

Performance Prediction: The data from stress and strain tests can be used to create models that predict how materials will behave under different conditions. This aids in simulating and optimizing performance in various applications.

In summary, maximum stress and strain tests are instrumental in ensuring the safety, reliability, and performance of materials and products across a wide range of industries. They provide critical data for design, quality control, and research and development efforts.

In Table 3, data is presented regarding the maximum stress levels at pinna positions A, B, C, D, and E. Notably, the highest stress value was observed at position E, measuring 1.08 MPa, while the lowest value was recorded at position A, measuring 0.33 MPa. This data is pivotal for evaluating the structural integrity and performance of the actuator under different configurations.

An in-depth analysis of the maximum stress values at each designated position provides a comprehensive understanding of how different actuator arrangements influence stress distribution across the pinna. This understanding is crucial for refining the design, ensuring that the actuator system not only achieves the desired deformation but also operates within acceptable stress tolerances. Ultimately, this contributes to enhancing the overall effectiveness and safety of the system.

Table 3: Maximum stress at pinna.

Position	Stress (MPa)
A	0.33
B	0.48
C	0.56
D	0.53
E	1.08

In Table 4, the maximum stress levels at distinct actuator positions—A, B, C, D, and E—are presented. Notably, the highest stress value was identified at position D, measuring 9.33 MPa, while the lowest value was documented at position A, measuring 1.34 MPa. This dataset is essential for evaluating the distribution of stress within the actuator system across various configurations.

An in-depth analysis of the maximum stress at each actuator position is instrumental in assessing the structural robustness and performance of the system. This examination plays a key role in refining the design to ensure that the actuator configuration not only achieves the desired deformation of the pinna but also operates within acceptable stress limits. Ultimately, this contributes significantly to enhancing the overall efficiency and safety of the system.

Table 4: Maximum stress at actuator.

Position	Stress (MPa)
A	4.47
B	4.73
C	1.34
D	9.33 (at very few nodes) it is up to 5MPa
E	1.58

Table 5 outlines details about the maximum strain levels at distinct pinna positions—A, B, C, D, and E. Notably, the highest strain value was observed at position E, measuring

0.72e-5, while the lowest value was documented at position C, measuring 0.322e-5. This data holds significance for evaluating the distribution of strain across the pinna in various configurations of the actuator system.

The analysis of maximum strain at each pinna position is integral for assessing the deformation and flexibility of the pinna under the influence of the actuator arrangement. This understanding is crucial for refining the actuator configuration, ensuring that the system achieves the desired pinna deformation while operating within acceptable strain tolerances. Such an analysis contributes to the optimization of the actuator design, balancing the effectiveness of pinna deformation with the structural integrity of the system for practical applications.

Table 5 : Maximum strain at pinna.

Position	Strain
A	0.36e-5
B	0.369e-5
C	0.322e-5
D	0.487e-5
E	0.72e-5

Table 6 details the maximum strain levels at different actuator positions—A, B, C, D, and E. Notably, the highest strain value was observed at position D, measuring 0.747e-4, while the lowest value was documented at position E, measuring 0.696e-5. This data is instrumental for evaluating the distribution of strain within the actuator system under various configurations.

A comprehensive analysis of the maximum strain at each actuator position is crucial for understanding the deformation and flexibility of the system. It plays a key role in refining the design to ensure that the actuator configuration not only achieves the desired pinna deformation but also operates within acceptable strain limits. This contribution is vital for enhancing the overall efficiency and safety of the system.

Table 6: Maximum strain at actuator.

Position	Strain
A	0.29e-4
B	0.397e-4
C	0.112e-4
D	0.747e-4
E	0.696e-5

Table 7 presents critical information regarding the maximum displacement at various pinna positions, denoted as A, B, C, D, and E. The highest displacement at pinna recorded at position C, measures 3.50E-04 (mm), while the lowest value, documented at position A, measures 7.03E-05 (mm).

This dataset is essential for gauging the magnitude of movement or shift occurring at each specified pinna position in direct response to the actuator system. An examination of the maximum displacement values at each pinna position serves as a pivotal metric in evaluating the overall flexibility and responsiveness of the pinna to the applied forces emanating from the actuator arrangement. This dataset plays a crucial role in the iterative refinement of the actuator design, ensuring that the system achieves the intended pinna deformation while adhering to acceptable displacement limits. Moreover, it serves as a valuable tool in the optimization of the actuator configuration for practical applications, considering both the efficacy of pinna deformation and the dynamic responsiveness of the pinna to the applied forces from the actuator system.

Table 7: Maximum displacement at pinna.

Position	Displacement (mm)
A	7.03E-05
B	1.89E-04
C	3.50E-04
D	1.67E-04
E	1.39E-04

The information presented in Table 8 plays a crucial role in refining the design to guarantee that the actuator system not only attains the intended pinna deformation but also functions within acceptable displacement limits. The highest displacement at actuator recorded at position D, measures 6.03E-03 (mm), while the lowest value, documented at position E, measures 1.39E-04 (mm). This analysis is indispensable for optimizing the actuator configuration, considering both the efficacy of pinna deformation and the dynamic movement of the system in response to applied forces.

Table 8: Maximum displacement at actuator.

Position	Displacement (mm)
A	2.90E-04
B	2.65E-03
C	8.10E-04
D	6.03E-03
E	1.39E-04

Figure 6 presents a comparison of actuators based on their maximum stress values. Where it found that the highest value in actuator 1 and the lowest value found in actuator 7. This data is crucial for evaluating the structural performance and stress distribution across different actuator designs within the system. By comparing the maximum stress levels among the actuators, you can gain insights into which design is better suited for handling the applied loads and achieving the desired pinna deformation.

This comparison helps in the selection and optimization of the actuator design that not only effectively induces pinna deformation but also operates within acceptable stress limits. It informs the decision-making process to identify the most suitable actuator configuration for practical application, considering both performance and structural considerations.

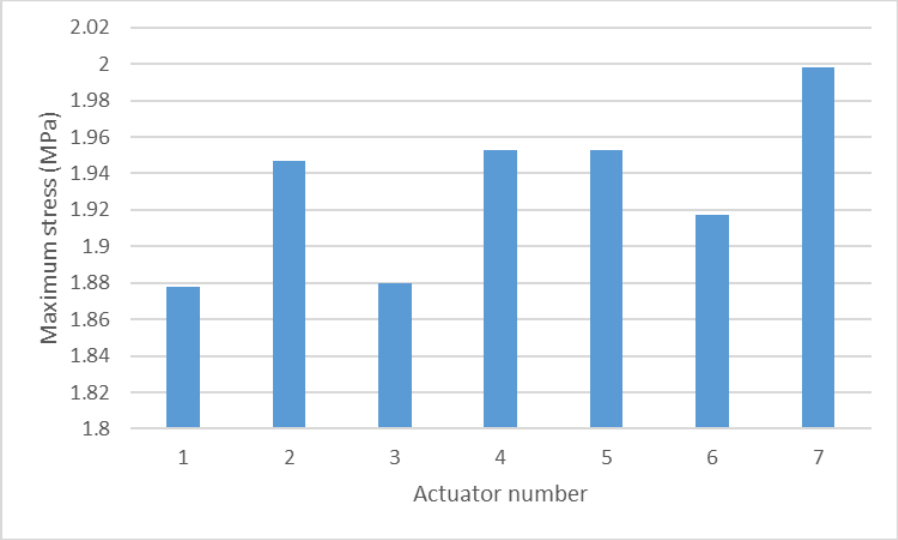

Figure 6: Maximum stress ranking for all the 7 actuators.

Table 9 shows optimizing meshing parameters for the pinna involves meticulous adjustments to capture fine details while balancing computational efficiency. Key considerations include determining an optimal element size, adjusting mesh density, implementing a boundary layer mesh, and ensuring overall mesh quality. This precision is vital for accurately representing the pinna's complex geometry in simulations. Simultaneously, configuring parameters for the five actuators demands strategic placement to ensure even force distribution, adjusting actuator strength for desired deformation, setting actuation frequency, and establishing control signals for synchronized operation. These parameters collectively contribute to the effective control

and response of the pinna to external stimuli. In parallel, parameters for equality checks, such as defining tolerance levels, convergence criteria, and verification metrics, are critical for validating simulation results. Fine-tuning these parameters ensures numerical accuracy and consistency, contributing to the reliability of the overall simulation and analysis.

Table 9: Meshing parameters for the pinna and 5 actuators.

Warpage	0
max aspect ratio	5
max skew angle	60
min tet collapse	0.1
min element length	0.01
maximum element length	2.33
minimum Jacobian	1
Details of elements (only pinna)	
number of elements	38045
number of nodes	10099
Element type	tetrahedral 4nodded (Solid 285)
Details of elements (arrangement1)	
number of elements	146747
number of nodes	35179
Element type	tetrahedral 4nodded (Solid 285)
Details of elements (arrangement2)	
number of elements	130306
number of nodes	30790
Element type	tetrahedral 4nodded (Solid 285)
Details of elements (arrangement3)	
number of elements	147167
number of nodes	34620

Element type	tetrahedral 4nodded (Solid 285)
Details of elements (arrangement4)	
number of elements	82305
number of nodes	19924
Element type	tetrahedral 4nodded (Solid 285)
Details of elements (arrangement5)	
number of elements	82305
number of nodes	19924
Element type	tetrahedral 4nodded (Solid 285)

The criterion for success is achieving a maximum deformation equal to or greater than 50% of the pinna's height, which, in this case, is 50 mm. Thus, the target deformation is set at 12.5 mm. Figure 6 provides an overview of the results from various arrangements. Where there are 5 different arrangements labelled (a), (b), (c), (d), and (e) of actuators with respect to pinna.

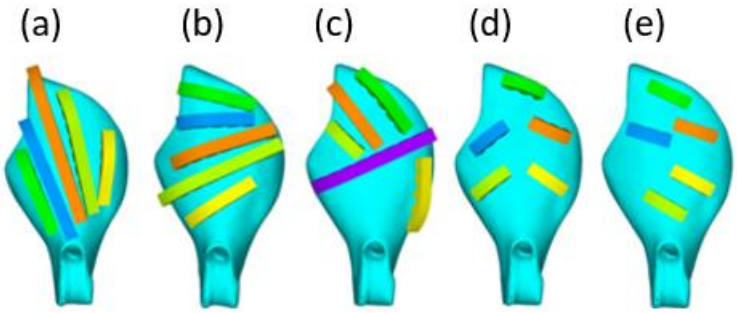

Figure 7: Summery of pinna arrangements deflection before applying the load.

Figure 8 illustrates the deflection distribution across five pinna arrangements in the model, labeled (a), (b), (c), (d), and (e). The maximum deflections for these arrangements were recorded as (9.89), (7.63), (9.53), (13.6), and (13.8), respectively, all measured in millimeters. As Arrangements D and E exceed the specified deformation threshold, meeting the required criteria, they are considered successful. With this success, the next step involves determining the optimal configuration through Design Space exploration. This exploration entails analyzing various configurations to identify the most effective arrangement for achieving the desired pinna deformation. The objective is to refine and optimize the actuator configuration for practical application, taking into consideration factors such as stress distribution, performance efficiency, and overall effectiveness in inducing controlled pinna deformation.

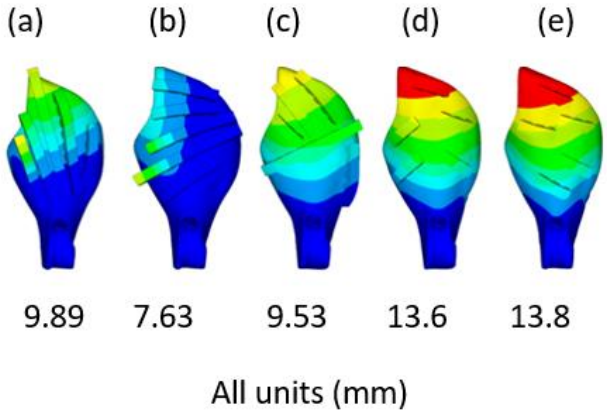

Figure 8: Summary of pinna arrangements deflection.

4.3 Design space of actuators configurations

The design space employed for optimizing actuation patterns, illustrated in Figure 9, involves the strategic positioning of five actuators (1-5) within a designated area on the pinna surface, as demarcated by dashed lines. Each actuator possesses the flexibility to vary in terms of position, angle (θ), and length (L). The quest for the optimal configuration orientations of these five actuators entails a systematic breakdown of parameters, plotted across different ranges. Specifically, the variation in angles spans between -15 to 15 mm, while the length ranges from 0 to 50 mm, providing a comprehensive exploration of potential configurations.

The optimization process entails the utilization of a code, outlined in Appendix A, which facilitates the generation of a set of five random parameters within the specified ranges. These parameters are then subjected to a scrutiny process involving a specific function named "ProgramTest." The function returns either true or false based on the

compatibility of the parameters with the desired criteria. The iterative nature of this process involves a continuous generation of new random parameters until the function yields a true result. The associated counter variable concurrently tracks the number of iterations necessary to identify a set of parameters that satisfy the function's criteria.

This systematic exploration of the design space, driven by the dynamic interplay of position, angle, and length parameters, is instrumental in honing in on configurations that optimize the actuation patterns for the five actuators. The iterative nature of the process, guided by the "ProgramTest" function, not only ensures the identification of viable parameter sets but also provides valuable insights into the efficiency and effectiveness of the actuation patterns within the specified constraints. This meticulous approach underscores the significance of computational techniques in achieving optimal configurations for intricate systems such as those involving pinna actuation.

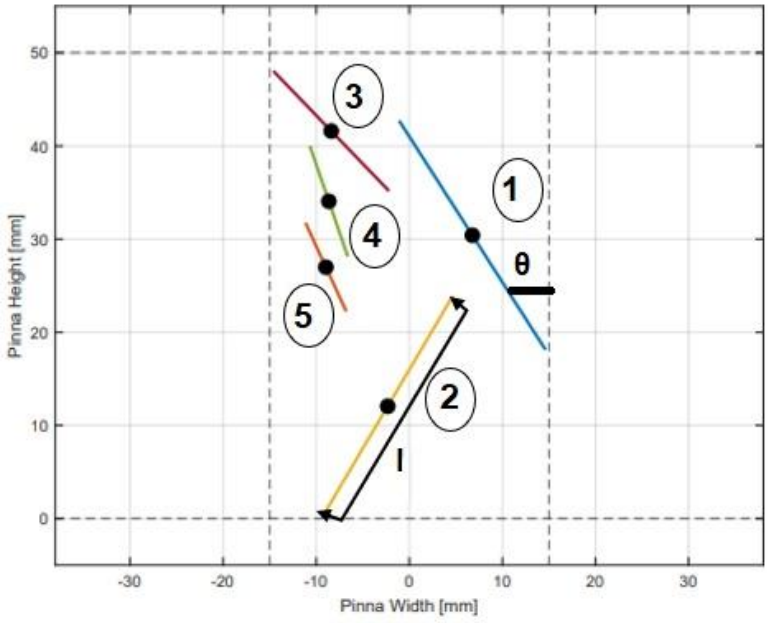

Figure 9: Design space used for the optimization of the actuation patterns.

The exploration of the design space has proven to be highly successful, accomplishing its primary objective of identifying diverse configurations. Through this iterative process, two distinct conceptual approaches have emerged: the parallel concept and the nonparallel concept. Each of these concepts represents a unique and innovative perspective within the design space, offering valuable insights into the potential configurations and variations that can be achieved. The parallel concept involves configurations where elements or components align in a parallel orientation, emphasizing a streamlined and cohesive arrangement. On the other hand, the nonparallel concept introduces configurations that deviate from parallel alignment, showcasing a more dynamic and unconventional arrangement. The coexistence of these two concepts not only expands the spectrum of possibilities within the design space but also opens avenues for further exploration and refinement. This duality in conceptual outcomes provides designers and researchers with a rich reservoir of options to

consider, fostering creativity and adaptability in the pursuit of optimal solutions within the defined design parameters. The success of the design space in generating these parallel and nonparallel concepts underscores its effectiveness as a tool for innovative ideation and configuration exploration in complex systems.

4.4 Actuators activation patterns.

Generate a comprehensive set of actuator activation patterns for a system comprising 5 actuators, with each actuator offering 3 distinct force levels. The total number of potential combinations amounts to 3^5, resulting in 243 conceivable configurations. Table 10 meticulously delineates the diverse force scenarios corresponding to both design space configurations, namely the parallel and nonparallel configurations.

Table 10: Scenarios for each design.

Scenario	Design
Scenario 1 force vector (0,1,2)	Design parallel
	Design nonparallel
Scenario 2 force vector (0,2,3)	Design parallel
	Design nonparallel
Scenario 3 force vector (0,1.5,3)	Design parallel
	Design nonparallel

In figure 10, the interrelation among the actuator number, activation pattern, and their corresponding force levels is depicted. The graphical representation illustrates the entire spectrum of potential combinations involving 5 actuators, each boasting 3 distinct force

levels. This visualization serves to enhance comprehension regarding the myriad force combinations and their consequential effects on the system.

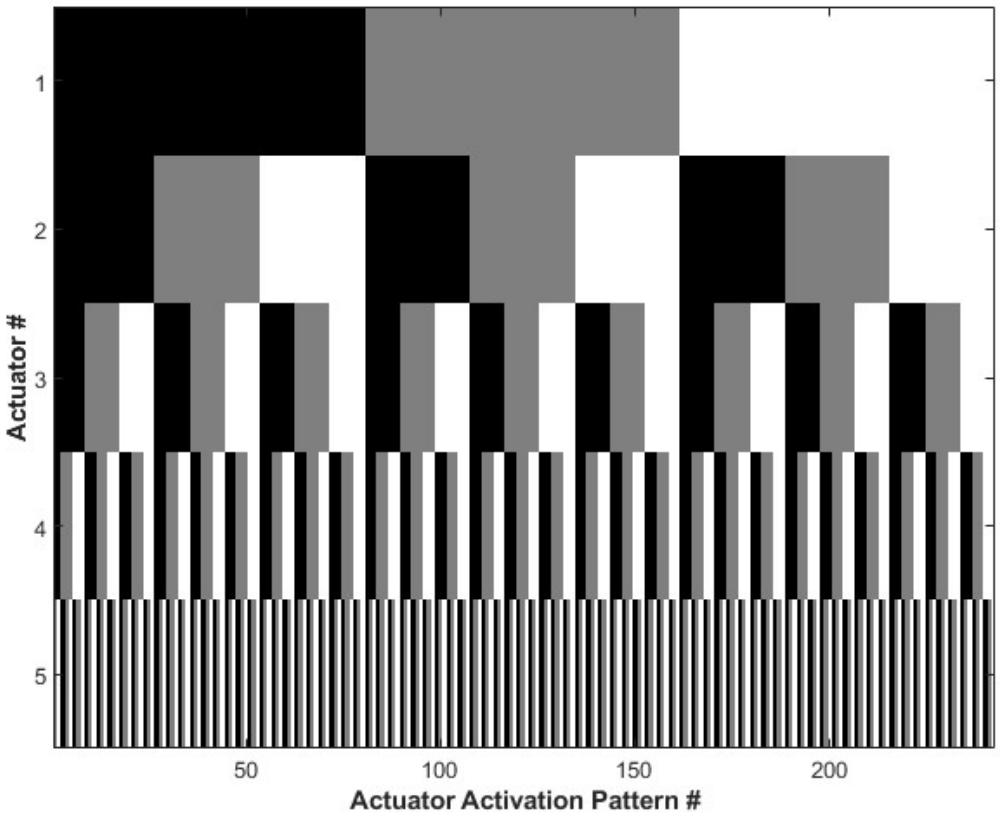

Figure 10: Actuators activation patterns.

A detailed examination was undertaken to explore the correlation between the actuator number and the force level associated with it across three distinct scenarios. Among these scenarios, the outcomes obtained from Scenario 3 proved to be particularly promising and impactful. As a result of the favorable results observed in Scenario 3, it has been discerningly chosen as the foundational basis for a more in-depth exploration through a Finite Element Analysis (FEA) parametric study. This strategic decision aims to leverage the insights gained from Scenario 3, ensuring a comprehensive investigation into the intricate interplay between actuator numbers and their corresponding force levels, thereby contributing to a more nuanced understanding of the system dynamics. The selection of Scenario 3 as the focal point for the FEA parametric study underscores its potential significance in unraveling key insights for the optimization and refinement of the overall system.

Chapter 5 FEA numerical simulation

5.1 Material characterizations.

The exploration and determination of material mechanical properties stand as a foundational and integral component of the research endeavor. This multifaceted initiative involved a thorough investigation into the inherent characteristics of the material employed in the study. Employing a combination of experimental procedures and analytical techniques, essential mechanical properties were meticulously extracted, contributing to a holistic understanding of the material's behavior across diverse conditions.

Undoubtedly, the identified material characteristics serve as fundamental input parameters for Finite Element Analysis (FEA) simulations. These properties furnish crucial insights guiding the material's behavior within the simulated environment, allowing for precise predictions of its responses under varying loading conditions. FEA simulations, rooted in mathematical models that replicate the physical behavior of the material, heavily rely on accurate material properties to generate meaningful and reliable results. The meticulous determination of these material characteristics not only informs the simulation models but also establishes a robust foundation for the extrapolation of real-world behavior and responses of the material in complex scenarios.

5.1.1 Material selection for the actuators

To meet the elasticity requirements, the material under consideration must exhibit a nonlinear nature. Hyperelastic materials, known for their softness, nonlinearity, hyperelastic deformation, complete energy recoverability, and either heavy or full incompressibility, emerge as particularly relevant. In alignment with the second law of thermodynamics, the material options under scrutiny encompass Ecoflex 50 and Dragon skin 30. While Ecoflex 50 was readily available in Ansys, Dragon skin 30 initially lacked representation. Consequently, tests were conducted on Dragon skin 30, with a specific focus on the tensile test due to the material's sensitivity to thickness variations. A strain of 150% was identified as imperative to fulfill the fundamental requirement of achieving a 150% deformation. This meticulous exploration and testing process aimed to ensure that the material properties align with the desired nonlinear characteristics essential for the elasticity criteria.

5.1.2 Manufacturing and testing process

The experimental procedure commenced with the creation of a 3D model for the specimen utilizing Fusion 360 CAD software, as visually represented in Figure 11.

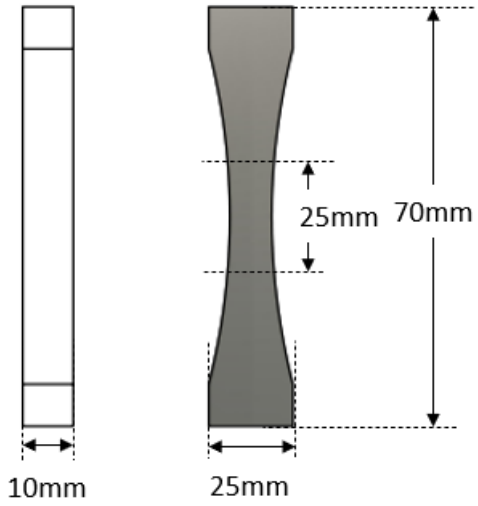

Figure 11: Specimen dimensions.

Following this design phase, test samples were fabricated through 3D printing, employing both Fused Deposit Modeling (FDM) and Stereolithography (SLA) technologies. To facilitate this fabrication process, molds were meticulously crafted using plastic boxes, yielding a minimum of 5 molds, as portrayed in Figure 12.

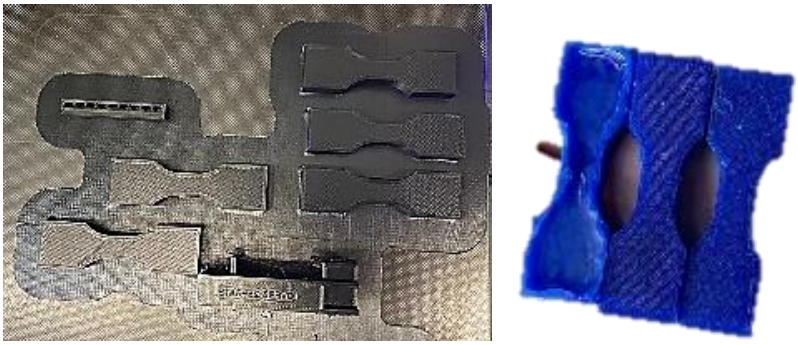

Figure 12: 3D printing samples

These molds were then filled with Dragon skin 30, a two-part material consisting of part A for strength and part B as the binding factor, maintaining a precise mixing ratio of

1:1. Precision in material preparation was upheld by carefully weighing and combining 150 g of each part A and B in a cup, followed by the addition of pigment to ensure the correct ratio. To prevent adhesion with the mold, a strategic layer of clay was placed beneath the specimens. Subsequently, a vacuum machine was employed for 8 minutes, after which the molds were left to dry for approximately 5 hours. The 3D-printed specimens were then delicately removed, and before reusing Dragon skin, a specialized spray was applied to the molds to prevent adhesion.

In the final step of this intricate process, the molds underwent an additional 8 minutes of vacuum treatment. This meticulous and multi-step procedure ensured the successful production of specimens endowed with consistent material properties, laying the foundation for subsequent testing and in-depth analysis. The integration of various technologies, precise material mixing, and attention to preventing adhesion guaranteed the reliability and reproducibility of the fabricated specimens for rigorous testing and analytical endeavors.

The experimental configuration featured the utilization of the Instron 4204 machine, complemented by the MTS control system. As depicted in Figure 13, the test machine played an active role throughout the experiment, capturing the state of the test sample post-failure. Notably, an Extensometer was omitted from the strain measurement process due to its limited capacity to calculate strains only up to a maximum of 50%. In response to this limitation, a Digital Caliper was employed as an alternative tool, ensuring precise and accurate strain measurements.

To maintain consistency in the applied force, a constant load of 1 kN was upheld throughout the experimental trials. The endpoint speeds of the machine varied, ranging from a minimum of 0.1 mm/min to a maximum of 200 mm/min. However, a deliberate choice was made to set the speed at 25 mm/min for the experimental procedure to ensure a high level of accuracy. This careful selection of speed played a pivotal role in generating precise stress load calculations, considering the cross-sectional area and facilitating the accurate determination of strain.

The systematic and meticulous approach adopted in this experiment was geared towards ensuring the acquisition of reliable and precise data. This commitment laid the groundwork for a robust and credible foundation for subsequent analyses, providing a solid basis for drawing meaningful conclusions from the experimental outcomes. The integration of alternative measurement tools and the careful selection of experimental parameters underscore the methodical nature of the experimental design, contributing to the accuracy and trustworthiness of the obtained data.

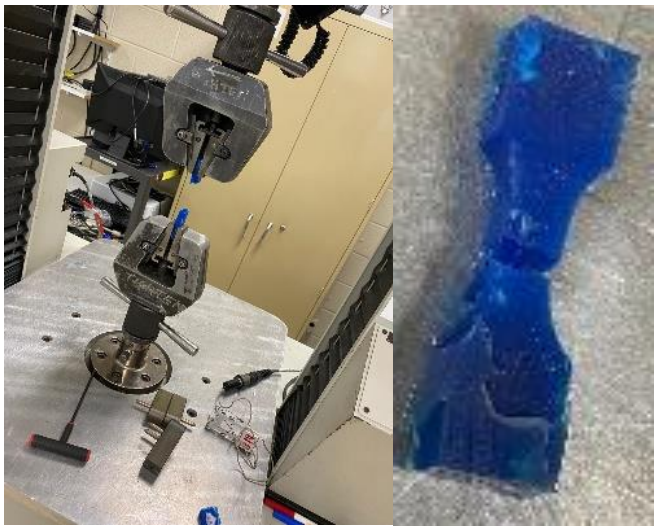

Figure 13: Test machine and sample after failure.

Figure 14 offers a visual representation of the Young's Modulus analysis conducted on Dragon skin 30, presenting the data in the format of Engineering Stress over Engineering Strain. It is imperative to underscore that, throughout this analysis, the cross-sectional area remains constant, signifying that it undergoes no alterations during the entirety of the experiment. This assumption of a static cross-sectional area allows for a concentrated examination of the material's behaviour in response to stress relative to strain, disregarding any potential variations in cross-sectional dimensions. This focused analysis contributes to an enhanced understanding of the material's mechanical properties and its ability to withstand stress under consistent cross-sectional conditions. By maintaining the cross-sectional area constant, the analysis provides insights into the intrinsic behaviour of Dragon skin 30, fostering a more nuanced comprehension of its mechanical responses in the face of stress-induced deformations.

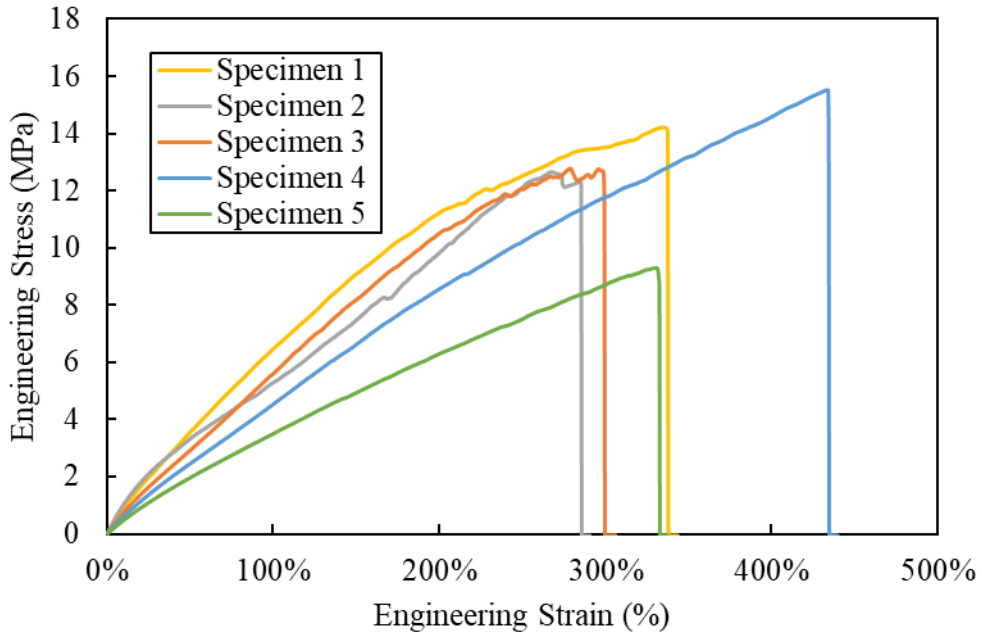

Figure 14: Engineering stress and strain for the 5 test samples.

Figure 15 illustrates the outcomes of the Young's Modulus analysis conducted on Dragon skin 30, presenting data in the format of True Stress over True Strain. A distinctive feature of these results is their enhanced realism, attributed to the dynamic consideration of the cross-sectional area, which undergoes changes over time. In contrast to a static cross-sectional area, this approach aligns with the actual behavior of the material during deformation, offering a more accurate depiction of its response to stress and strain. The equation employed for deriving these outcomes accommodates the evolving nature of the cross-sectional area, providing a more realistic representation of Dragon skin 30's mechanical behavior under conditions where the cross-sectional area is not static but dynamically evolves throughout the analysis. This dynamic consideration contributes to a more nuanced and authentic understanding of the material's response to varying stress and strain conditions.

`True strain = ln(1 + engineering strain)` where ln designates the natural log

`True stress = (engineering stress) * exp(true strain) = (engineering stress) * (1 + engineering strain)`

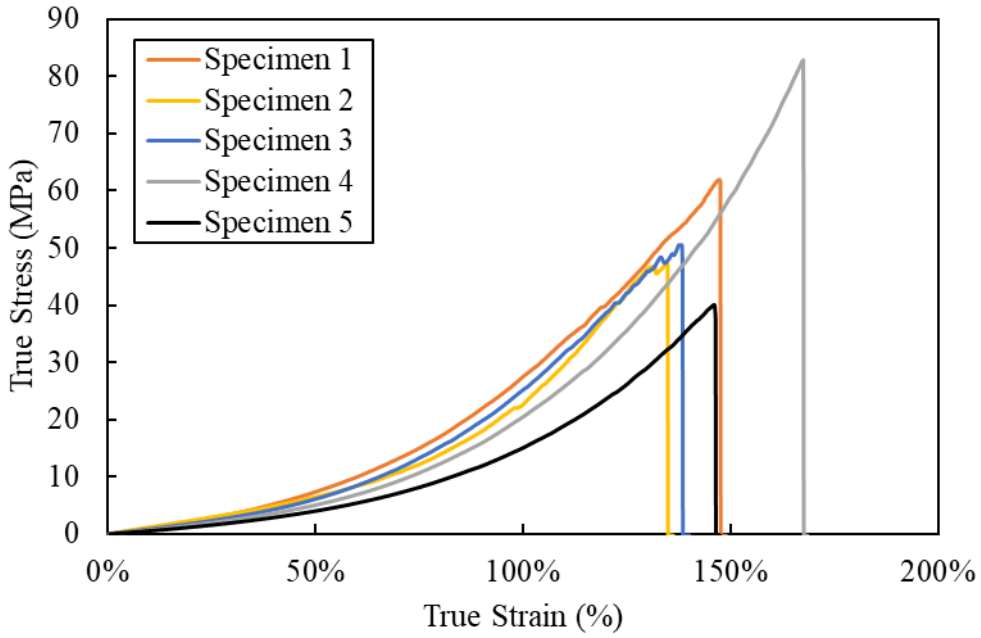

Figure 15: True stress and strain for the 5 test samples.

A noteworthy observation is that the expected strain value aligns closely with the targeted 150%, in accordance with the specified requirement for achieving a 150% deformation. This underscores the material's response in meeting the prescribed deformation goal. The utilization of the True Stress/True Strain framework, coupled with the dynamic consideration of the cross-sectional area, contributes to the heightened accuracy of the analysis. This approach imparts insights that closely parallel real-world behavior, enhancing the reliability and authenticity of the obtained results.

Figure 16 shows the mechanical attributes of Ecoflex 50 elucidated through a comprehensive examination, encompassing results obtained from a range of tests including uniaxial, biaxial, and shear assessments. In the realm of uniaxial testing, Ecoflex 50's behavior under unidirectional stress is scrutinized, providing insights into its tensile or compressive strength, elastic modulus, and strain at failure. Moving beyond uniaxial tests, biaxial evaluations delve into the material's response to stress applied along two perpendicular axes, offering a more holistic understanding of its mechanical performance. Additionally, shear tests explore Ecoflex 50's resistance to forces acting parallel to its surfaces, providing crucial data on its shear modulus, and yielding behavior under shear stress. This multifaceted examination not only enhances our comprehension of Ecoflex 50's mechanical properties but also ensures a more nuanced and accurate representation of its behavior across various loading conditions.

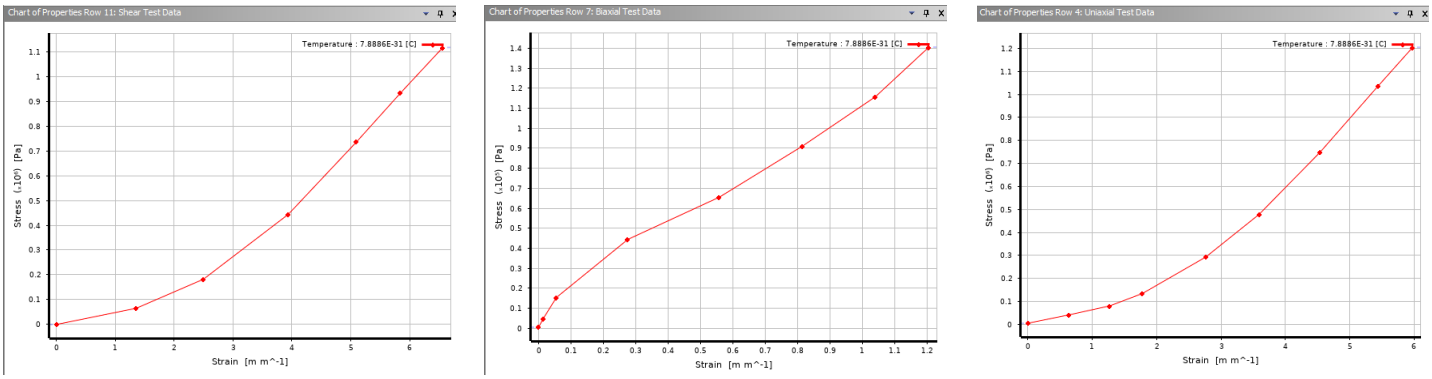

Figure 16: Mechanical properties of Ecoflex 50.

Table 11 provides an extensive juxtaposition of Ecoflex 50 and Dragon skin 30, delineating crucial parameters and characteristics that differentiate the two materials. This comparative analysis spans diverse facets, encompassing mechanical properties and other pertinent factors, contingent upon the specific context of your research or application. Individual rows in the table correspond to distinct attributes, with dedicated columns for Ecoflex 50 and Dragon skin 30, facilitating a side-by-side assessment of their respective qualities.

Table 11: Comparison between Ecoflex 50 and Dragon skin 30.

Property	Ecoflex 50	Dragon skin 30
Softness/Flexibility	High, known for soft and flexible nature	Flexible, with some formulations mimicking the feel of human skin
Shore Hardness	Available in various shore hardness ratings	Formulations with specific shore hardness
Tear Strength	Good tear strength	High tear strength, durable and resilient
Transparency	Some formulations may have transparency	Transparency may vary based on formulations
Paintability	Generally paintable	Paintable, allows for detailed customization
Chemical Resistance	Specific formulations may vary in resistance	Generally, exhibits good chemical resistance
Special Features	- Versatile in hardness options	- Mimics skin feel in some formulations
	- Soft and pliable for diverse applications	- High tear strength for durability

5.2 Actuation system control

In the realm of engineering and technology, the design and implementation of control systems are critical for achieving precision, efficiency, and desired outcomes across a wide array of applications. The choice of a mini control system, a compact and integrated solution, has gained significant attention due to its potential to provide effective control in constrained spaces, lightweight platforms, and applications demanding portability. The selection of a mini control system involves a detailed evaluation of factors such as size, computational power, real-time processing capabilities, and energy efficiency. This introduction delves into the considerations and advantages that underpin the decision to opt for a mini control system, outlining the relevance and impact of this choice across diverse industries and domains. As technological advancements continue to push the boundaries of innovation, the judicious selection of a mini control system emerges as a strategic decision to enhance system performance and meet the evolving demands of modern applications.
An important fact the control system required must produce force to the required work. There are several servos are discussed below:

RE25, Maxon Motor AG: This servo model is associated with Maxon Motor AG and falls within their RE25 range. Specific performance characteristics and applications would depend on the detailed specifications of this model.

D930SW Servo: This servo from an unspecified manufacturer and model range carries the designation "D930SW." The features and capabilities of this servo would be defined by its manufacturer's specifications.

D940TW Servo-Clockwise (stock)-Stock Rotation: This servo, known as the D940TW, has a clockwise rotation and comes from an undisclosed manufacturer. The name suggests that it has a stock rotation orientation.

2000 Series Dual Mode Servo (25-4, Super Speed): A servo belonging to the 2000 Series and featuring dual-mode functionality, offering a Super Speed mode. The "25-4" identifier might pertain to specific torque or size characteristics of this servo.

SC1258TG-BE Standard Size Coreless Digital Servo: This is a standard-sized servo with a coreless digital design, identified by the model number SC1258TG-BE. The specifics of torque, speed, and other attributes would be defined by the servo's manufacturer.

Figure 17 provides a visual representation of the 99 Micro Servo. The specifications of the 99 Micro Servo, emphasizing its suitability for applications requiring a combination of high torque and speed within a compact form factor. Notable features such as its waterproof design, precision metal gears, and robust aluminum case contribute to its versatility, rendering it suitable for use in various scenarios where environmental

conditions may be a concern. The availability of torque and speed options across different voltage levels further enhances its adaptability for diverse applications.

Figure 17: An image for the 99 Micro Servo (from Reefs RC, 2023).

Table 12 succinctly outlines the key specifications of the "99 Micro Servo," providing a comprehensive overview of its features, performance characteristics, and technical

details. Additionally for detailed specifications of all other servos, please refer to Appendix D.

Table 12: Specifications of the 99 Micro Servo (from Reefs RC, 2023).

Specification	Value
Type	High torque, high-speed micro servo
Waterproof	Yes
Operating Voltage Range	6V - 8.4V
Gears	Precision metal gears
Case Material	All CNC aluminum REEFS case
Bearing System	2-ball bearing system
Weight	Approximately 0.70 ounces
Dimensions (L x W x H)	0.90" x 0.47" x 1.08" (L x W x H)
Torque (at different voltages)	89 oz-in at 6.0V
	99 oz-in at 7.4V
	115 oz-in at 8.4V
Speed (per 60 degrees at various voltages)	0.11 sec at 6.0V
	0.09 sec at 7.4V
	0.08 sec at 8.4V
Spline	25T Micro
Dead Band Width	2 microseconds (µs)
BEC Requirement	Not required

5.2.1 Tendon routing calculations

This is the methodology of how to calculate the force required for tendon routing based on pulley-servo torque measurements, the following formula can be used:

$$Tc=\eta Fa\cdot r1$$

Tc is the torque required during constant velocity (Nm).

Fa is the total axial force (N).

$r1$ is the radius of the drive pulley (mm).

η is the efficiency of the belt drive system.

Given that the radius $r1$ is 35 mm and the expected efficiency η is 0.9, and that the total torque is calculated as 90% of the torque from the pulley, the equation can be rearranged to solve for Fa:

$$Fa = r1Tc \cdot \eta$$

Plugging in the values:

$$Fa = 0.9 \cdot T\text{pulley} \cdot 0.9/35$$

Where, Tpulley is the torque from the pulley.

This will give you the total axial force Fa required for tendon routing based on the given torque measurements and system efficiency.

5.3 FEA model

This section involves the development of Finite Element Analysis (FEA) models for the actuators, enabling a comparative evaluation across the seven distinct concept designs depicted in Figure 1. These designs encompass both parallel and nonparallel configurations, as illustrated in Figure 18, derived from the Design space. The forces applied to the models were determined based on the actuator activation patterns. After testing various materials, Ecoflex 50 was identified as the optimal choice. With the material selected, the subsequent step involves conducting a parametric study to further refine and analyze the system.

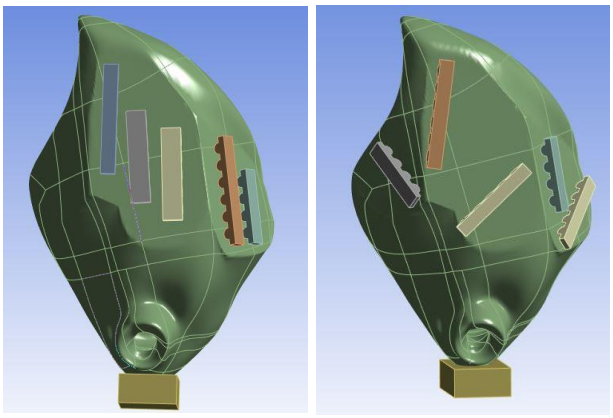

Figure 18: Parallel and nonparallel configurations.

5.3.1 Hyperplastic model

Like the initial Yeoh model, the second Yeoh hyperplastic model is commonly employed in finite element simulations to forecast the mechanical response of materials under various loading conditions. This is particularly useful for materials displaying pronounced nonlinear and strain-dependent behavior. The model parameters are typically fine-tuned through calibration using experimental data, ensuring a precise depiction of the material's hyperplastic properties, as exemplified in Figure 19.

Properties of Outline Row 3: Ecoflex 50

	A	B	C
1	Property	Value	Unit
2	Material Field Variables	Table	
3	Density	1131	kg m^-3
4	Uniaxial Test Data	Tabular	
5	Scale	1	
6	Offset	0	Pa
7	Biaxial Test Data	Tabular	
11	Shear Test Data	Tabular	
12	Has Lateral Strain	No	
13	Scale	1	
14	Offset	0	Pa
15	Yeoh 2nd Order		
16	Material Constant C10	18441	Pa
17	Material Constant C20	614.04	Pa
18	Incompressibility Parameter D1	0	Pa^-1
19	Incompressibility Parameter D2	0	Pa^-1

Figure 19: Hyper elastic model.

5.3.2 Meshing

Within the realm of meshing, the selection of an optimal element size holds paramount importance for ensuring precision and efficiency in simulations. Figure 20 provides a visual representation of coverage tests undertaken to ascertain the most suitable element size. The results of these tests conclusively demonstrated that an element size of 3 mm proved to be optimal, yielding a mesh with 1465 nodes.

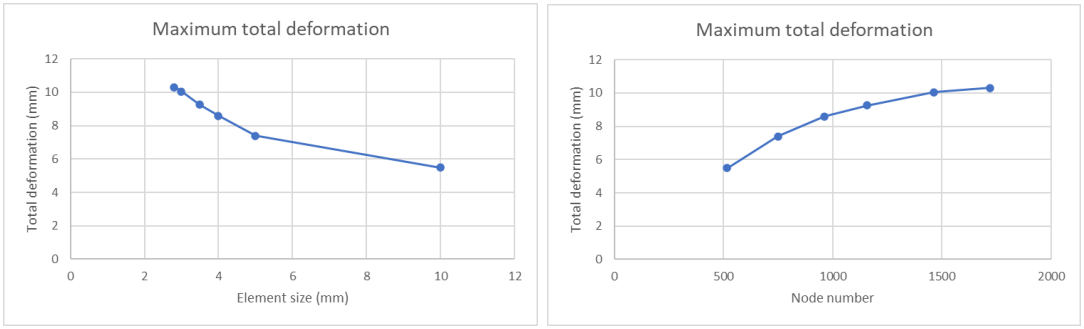

Figure 20: Meshing test samples.

The selected element size stands as a pivotal parameter in finite element analysis (FEA) simulations, exerting a significant impact on the mesh's level of detail. Striking a balance is imperative, aiming for a mesh fine enough to encapsulate intricate model features while upholding computational efficiency. The decision to opt for a 3 mm element size reflects a judicious compromise that aligns well with the specific simulation requirements, factoring in considerations of both accuracy and computational resources.

The node count, totaling 1465 in this context, provides valuable insights into the mesh's granularity. A higher node count typically signals a finer mesh, and this granularity is crucial for ensuring fidelity in FEA results. The meshing process, where the chosen element size and node count play integral roles, significantly influences the precision of FEA outcomes.

Documenting these specific details regarding the meshing strategy contributes to transparency and reproducibility in the simulation process. The efficacy of the chosen mesh parameters can be further evaluated by comparing simulation results with experimental or expected outcomes, providing a comprehensive assessment of the simulation's reliability and accuracy. Figure 21 shows the parallel and nonparallel meshes.

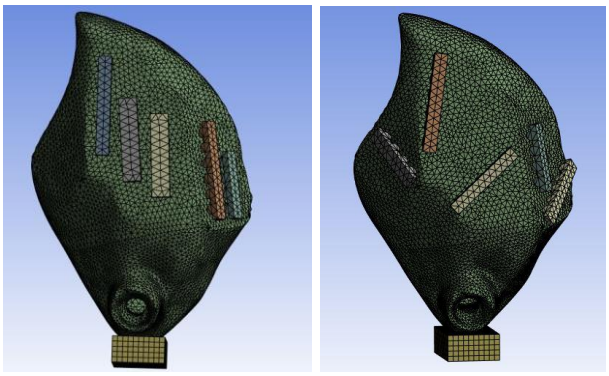

Figure 21: Parallel and nonparallel meshes.

5.3.3 Boundary conditions:

The set boundary conditions for this analysis entail a fixed base for all five actuators, illustrated in Figure 22 for parallel boundaries and Figure 23 for nonparallel boundaries. This implies that the base of each actuator is firmly restrained, simulating a scenario in which the actuators exhibit rigidity. This constraint mirrors real-world conditions where the base of the actuators remains anchored, facilitating the evaluation of their behavior and response to external loads.

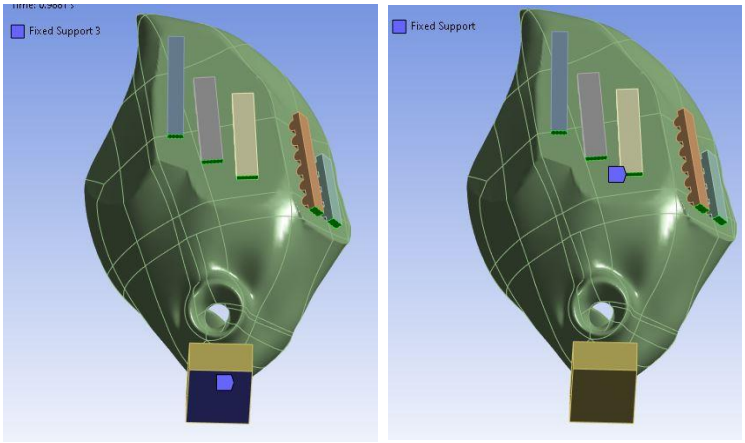

Figure 22: Parallel boundary conditions.

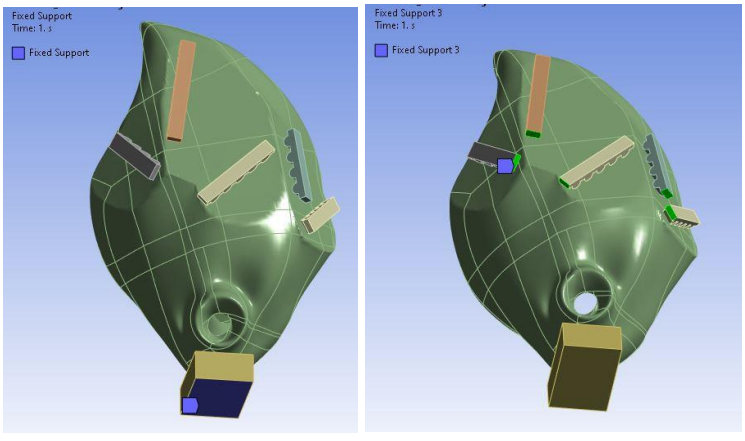

Figure 23: Nonparallel boundary conditions.

- **Fixed support-** All Degrees of Freedom are fixed at the actuator bottom face and base plate.
- Pinna: fixed base of the pinna, indicating that the base of the pinna is immobilized.
- Actuators: fixed base for all five actuators, implying that the base of each actuator is held in place.

5.3.4 Contacts

In the context of finite element analysis (FEA) or mechanical simulations, a bonded contact implies that the specified surfaces are constrained to move together as if they were a single entity. In this case, the actuators and the pinna are joined together in a manner where they share the same displacement or deformation, as if they are physically bonded or connected. This type of contact is often employed in simulations to model situations where components are rigidly attached, with no relative motion allowed between them. Figure 24 shows the bonded contacts provided between the 5 actuators and the pinna" indicates that in the presented schematic or visualization (Figure 18), a representation of a bonded contact between five actuators and the pinna is depicted.

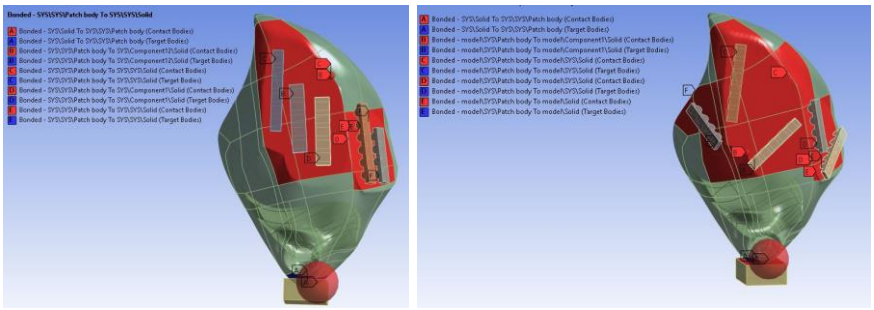

Figure 24: Parallel and nonparallel contact.

- Bonded contacts are provided between the components.

5.3.5 Loading conditions:

In terms of loading conditions, the analysis encompasses three distinct load scenarios, each applied at the head of the actuators:

- **Load: 0.000001N:** This represents a scenario with no applied load, serving as a baseline assessment to understand the inherent behavior of the actuators in the absence of external forces.
- **Load: 1.5N:** A load of 1 N is applied at the head of the actuators. This allows for the examination of their response to a relatively low force input.
- **Load: 3N:** The actuators are subjected to a load of 3 N at their heads, simulating a more significant external force to evaluate their performance under higher stress conditions.

By imposing these loading conditions, the analysis seeks to elucidate the reactions, deformations, and stress distributions exhibited by the actuators under varying levels of external loads. The amalgamation of fixed boundary conditions and diverse loading scenarios offers a holistic understanding of the mechanical behavior of the actuators,

ultimately informing design refinements and optimization endeavors, as depicted in Figure 25.

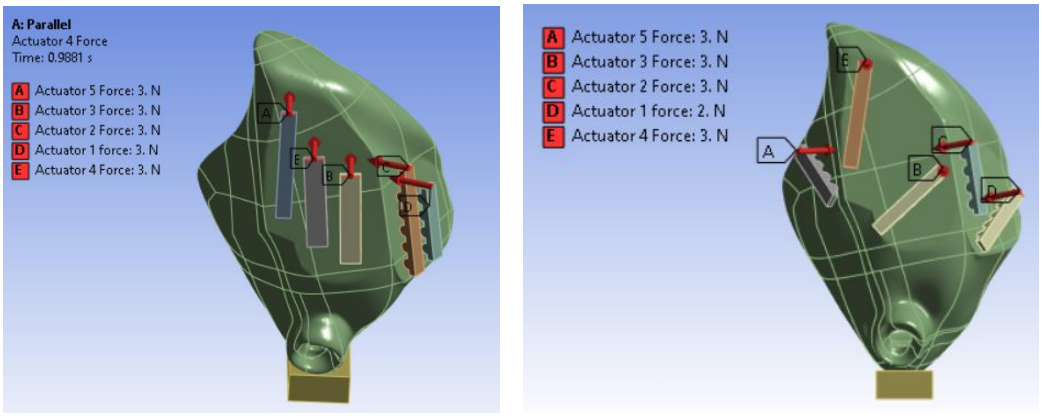

Figure 25: Parallel and nonparallel loading conditions.

5.4 FEA results

Figure 26 succinctly summarizes the parametric study, specifically focusing on parallel configurations. It features eight examples illustrating pinna deformation (1.0022, 2.0316, 3.5789, 4.4744, 5.4484, 6.2261, 7.3375, and 12.495)mm. The rationale behind showcasing these eight examples is to demonstrate the variety in results. These instances offer a snapshot of the study's outcomes, providing insights into the impact of parameter variations on pinna deformation within parallel setups. For a comprehensive view of the study's extensive results, covering 243 cases, please refer to Appendix I.

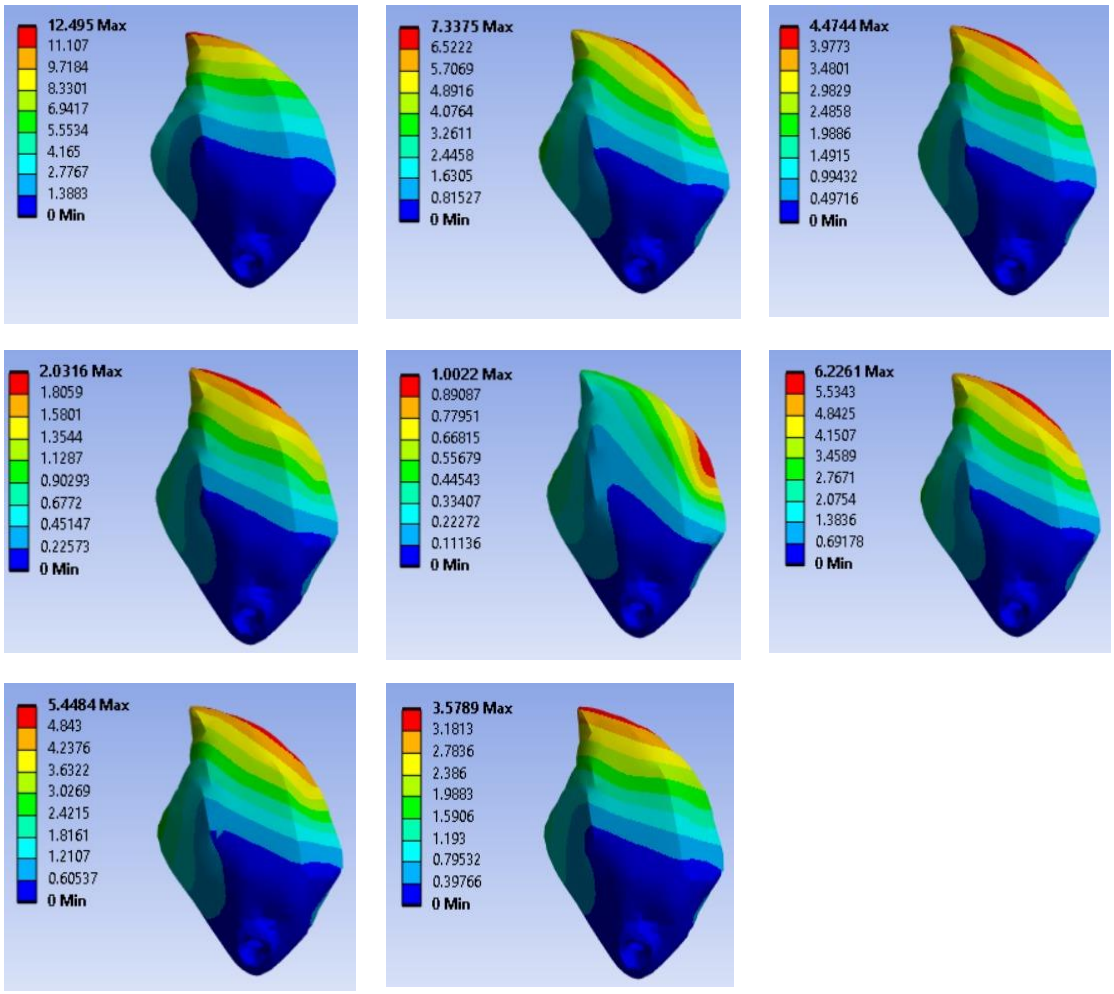

Figure 26: Parallel results (see Appendix I)

Figure 27 presents a summary of the parametric study focusing on nonparallel configurations. It displays eight examples of pinna deformation (7.2631, 8.9018, 4.6594, 4.6594, 9.5877, 6.4722, 4.8256, 2.478, and 11.408) mm. These examples serve as a concise representation of the study's findings, providing a snapshot of how variations in parameters impact pinna deformation. For a more detailed exploration, the extensive results of the study, comprising 243 cases, can be found in Appendix H.

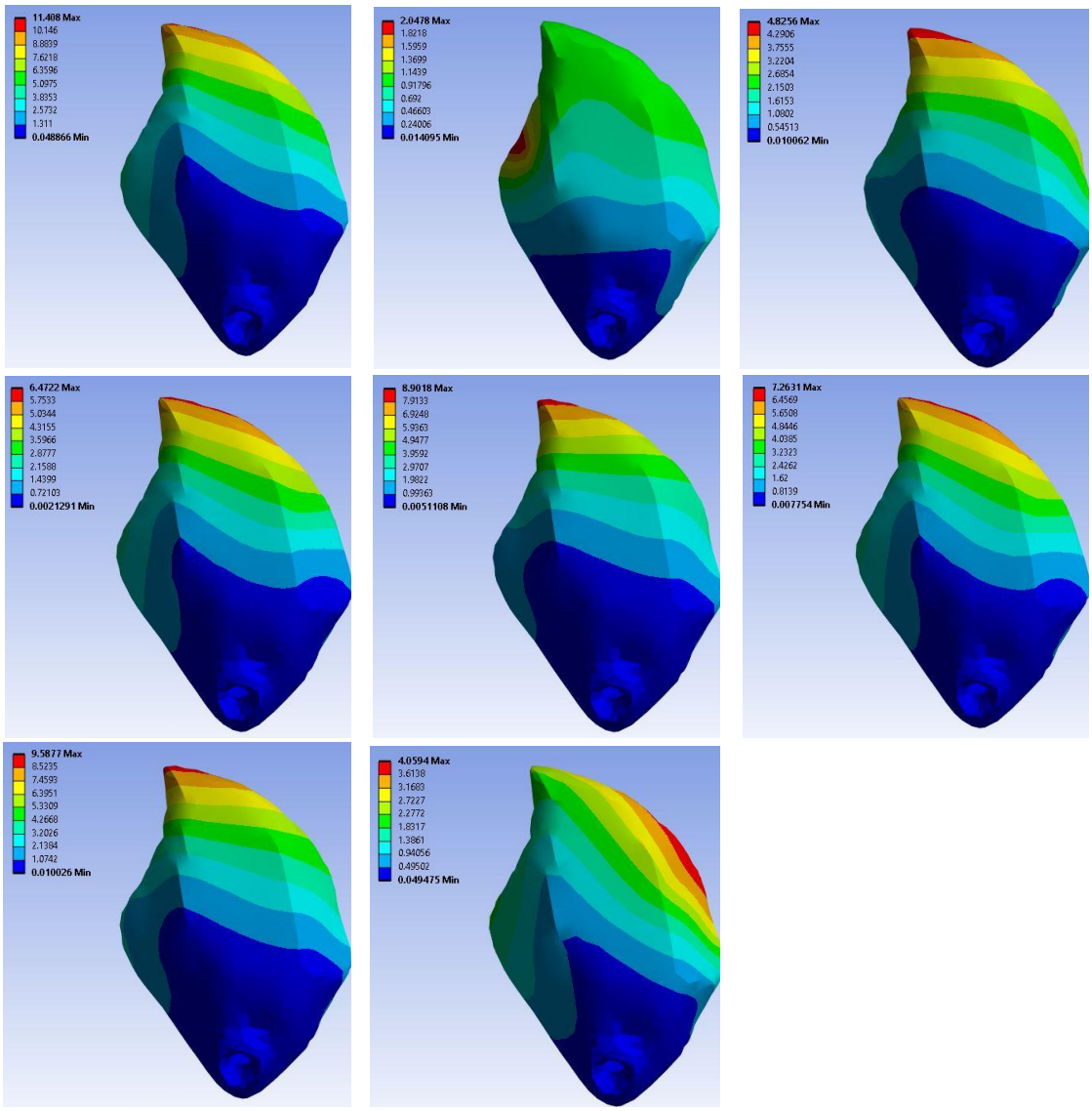

Figure 27: Nonparallel results. (See Appendix H)

Two tables were created through ANSYS to explore and comprehend the variations in pinna behavior, encompassing both parallel and nonparallel configurations. This information is visually represented in Figure 28, showcasing the results of parallel deformation for the pinna. It shows this that might be reachable and acceptable for the pinna deformation.

DP 236	3	3	1.5	1.00E-06	1.00E-06	9.305304438
DP 237	3	3	1.5	1.00E-06	1.5	10.89973254
DP 238	3	3	1.5	1.00E-06	3	12.49513466
DP 239	3	3	3	1.5	1.00E-06	10.41691131
DP 240	3	3	3	1.5	1.5	11.98424598

Figure 28: Parallel deformation results.

Figure 29 illustrates the outcomes of nonparallel deformation for the pinna. It shows this that might be reachable and acceptable for the pinna deformation.

DP 239	3	3	3	1.00E-06	3	3.743585239
DP 240	3	3	3	1.5	1.00E-06	7.60056282
DP 241	3	3	3	1.5	1.5	6.947612527
DP 242	3	3	3	1.5	3	6.348268124
DP 243	3	3	3	3	1.00E-06	11.3306077

Figure 29: Nonparallel deformation results.

A total of 123 nodes were considered, and for each node, the total deformation and corresponding forces were recorded. These tables are intended for use in Principal Component Analysis (PCA) and are attached in the appendix H and I.

5.5 FEA model analysis

Modal analysis is a crucial tool for examining and validating designs across various applications, from aircraft frame components to wind or gas turbine blades and vehicle chassis. This analytical method holds particular importance for structures exposed to forces that could induce harmful or destructive resonant frequencies in the absence of damping. Resonance frequencies with low damping can result in significant vibrations even with minimal input force or energy.

Modal analysis, implemented in finite element analysis, dynamically calculates Eigenvalues (natural frequencies) and Eigenvectors (mode shapes) for structures. This information provides engineers with a comprehensive understanding of the dynamic behavior of structures, offering insights into natural frequencies representing the frequencies at which a body vibrates when subjected to external forces. Mode shapes, meanwhile, depict deflection patterns associated with specific natural frequencies, illustrating the relative displacement of structural components.

Modal participation factors gauge the interaction between modes and directional excitation, with larger values indicating a more substantial contribution to dynamic response. Effective mass factors reveal the amount of system mass involved in a mode in each excitation direction, expressed as a percentage of the total system mass. Cumulative mass, which represents the sum of effective mass factors for specific modes, is instrumental in determining the predominant direction of excitation vibration and is commonly employed to guide the inclusion of modes in linear dynamic analysis.

Analysis set up

- Initial sub step -30
- Minimal Sub step-30
- Maximum sub step-50

Note: - The above iteration sub step setting is fine-tuned based on the convergence study in simulations

- No Force is required for Modal analysis.
- Parallel - No of modes defined in analysis 700
- Nonparallel - No of modes defined in analysis 3000
- Frequency range is adjusted to reach the effective mass of 99%. It can be iterative approach to reach the required mass contribution for the structure assembly.

In Table 13, the modal results for both Parallel and Nonparallel configurations indicate that the natural frequency is consistently higher for parallel configurations across almost all mode numbers, ranging from 1 to 10. In the context of this analysis, the term "parallel" signifies the orientation where the actuator is placed parallel to the pinna. Detailed tables containing this information are appended F and G for reference.

Table 13: Models comparison table.

Parallel	Nonparallel

Tabular Data

	Mode	Frequency [Hz]
1	1.	70.272
2	2.	103.91
3	3.	154.04
4	4.	171.1
5	5.	193.02
6	6.	203.35
7	7.	241.54
8	8.	265.34
9	9.	268.91
10	10.	291.37

Tabular Data

	Mode	Frequency [Hz]
1	1.	68.135
2	2.	118.65
3	3.	141.86
4	4.	161.13
5	5.	163.95
6	6.	216.11
7	7.	237.34
8	8.	240.25
9	9.	259.65
10	10.	274.09

The bat ears exhibit deformation at frequencies around 10Hz, and upon conducting modal analysis Finite Element Analysis (FEA), it is observed that the first natural frequency for both Parallel and Nonparallel configurations exceed 10Hz. Examining the FEA results, it becomes evident that the natural frequency is consistently higher for most mode numbers in the parallel configuration. In this setup, where the actuator is placed in parallel series with the pinna, the structure demonstrates superior stiffness compared to the nonparallel actuator arrangement in the assembly. This suggests that the parallel configuration is more effective in providing structural stability, aligning with the observed deformation characteristics of bat ears at frequencies around 10Hz. Table 14 shows the mode shapes for parallel (990.28, 980.68, 877.82, 1522.5, 1850.7, and 2203.6) Hz and nonparallel (1012.1, 1086.1, 1017, 1443.5, 2608.6, 1398.2)Hz.

Table 14: Mode shapes for parallel and nonparallel

Parallel	Nonparallel
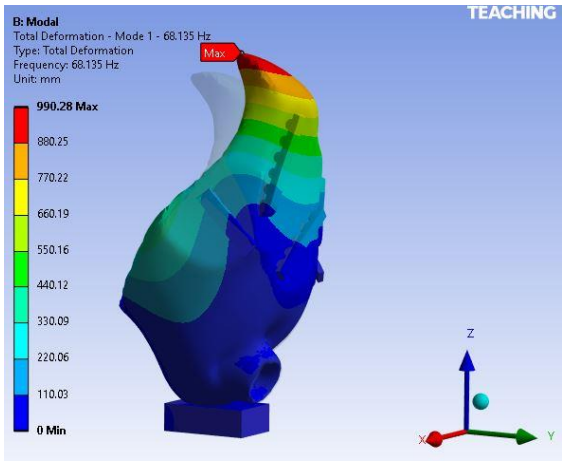	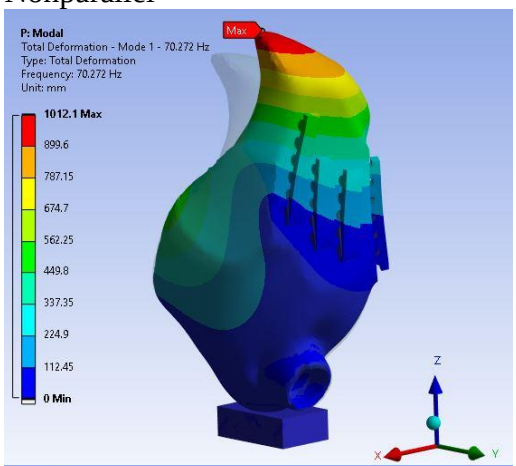
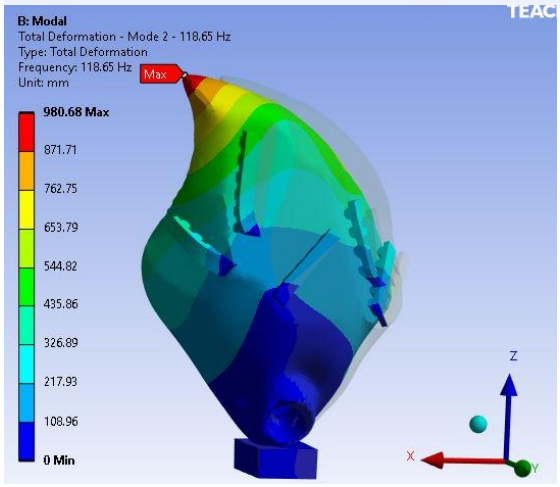	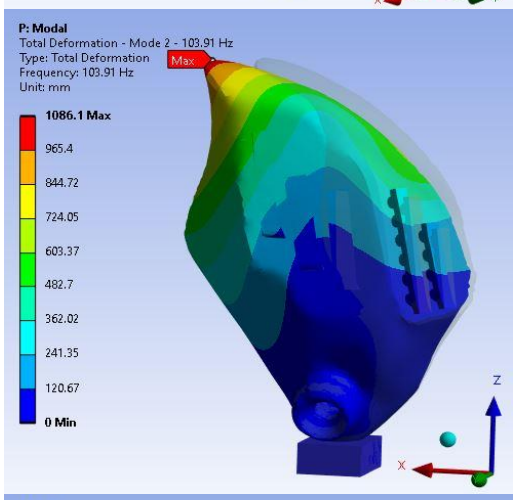
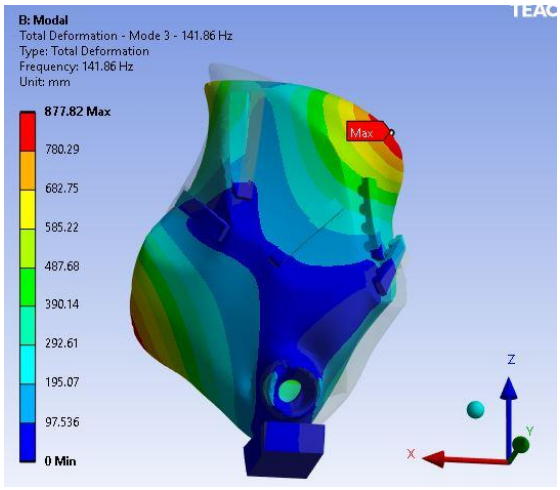	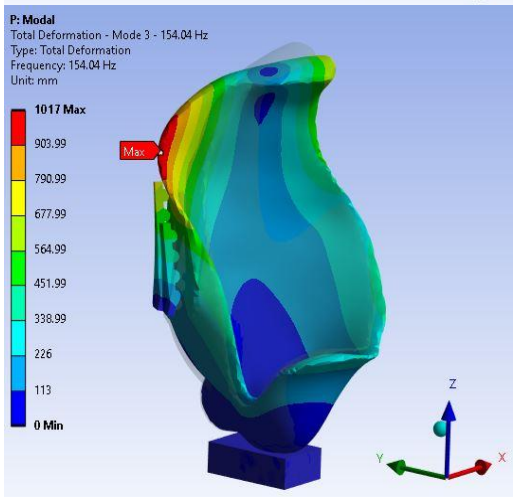

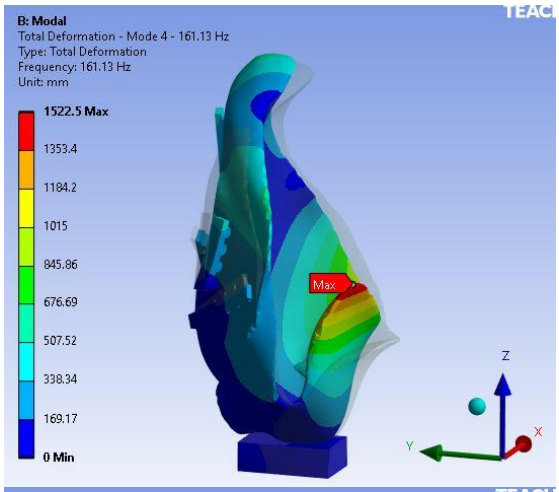
B: Modal
Total Deformation - Mode 4 - 161.13 Hz
Type: Total Deformation
Frequency: 161.13 Hz
Unit: mm
1522.5 Max
1353.4
1184.2
1015
845.86
676.69
507.52
338.34
169.17
0 Min
Max
Z
Y
X

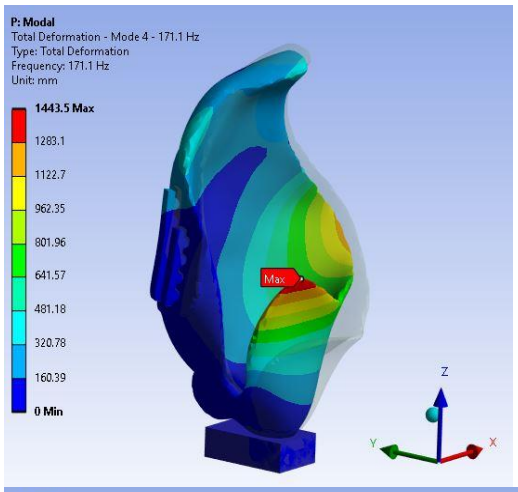
P: Modal
Total Deformation - Mode 4 - 171.1 Hz
Type: Total Deformation
Frequency: 171.1 Hz
Unit: mm
1443.5 Max
1283.1
1122.7
962.35
801.96
641.57
481.18
320.78
160.39
0 Min
Max
Z
Y
X

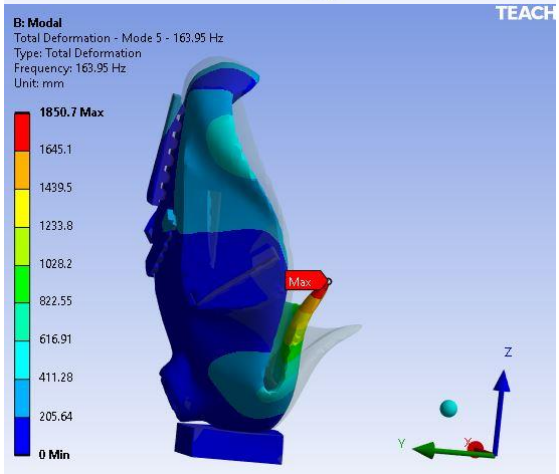
B: Modal
Total Deformation - Mode 5 - 163.95 Hz
Type: Total Deformation
Frequency: 163.95 Hz
Unit: mm
1850.7 Max
1645.1
1439.5
1233.8
1028.2
822.55
616.91
411.28
205.64
0 Min
Max
Z
Y
X

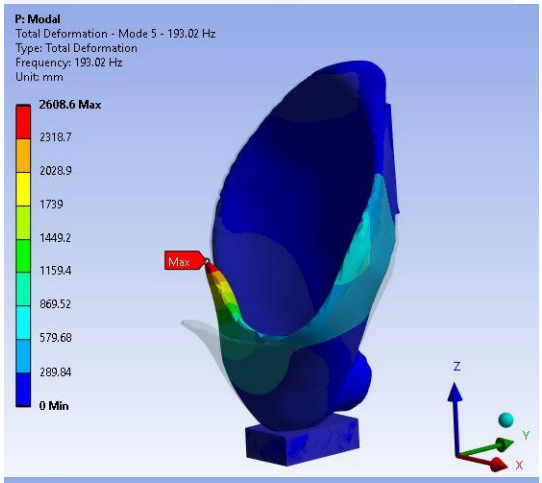
P: Modal
Total Deformation - Mode 5 - 193.02 Hz
Type: Total Deformation
Frequency: 193.02 Hz
Unit: mm
2608.6 Max
2318.7
2028.9
1739
1449.2
1159.4
869.52
579.68
289.84
0 Min
Max
Z
Y
X

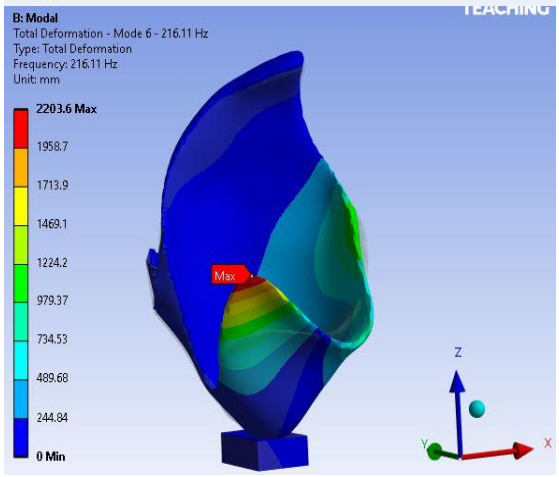
B: Modal
Total Deformation - Mode 6 - 216.11 Hz
Type: Total Deformation
Frequency: 216.11 Hz
Unit: mm
2203.6 Max
1958.7
1713.9
1469.1
1224.2
979.37
734.53
489.68
244.84
0 Min
Max
Z
Y
X

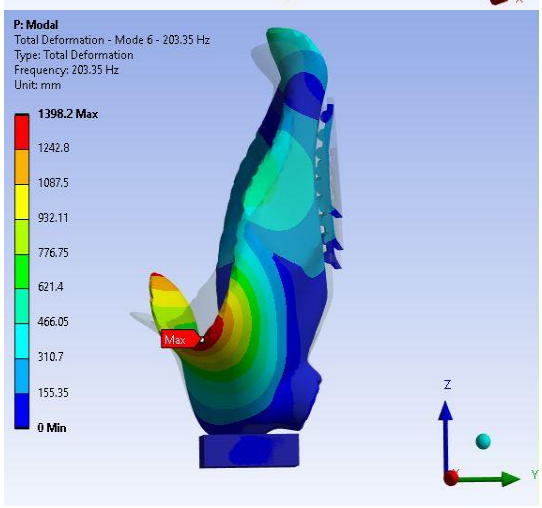
P: Modal
Total Deformation - Mode 6 - 203.35 Hz
Type: Total Deformation
Frequency: 203.35 Hz
Unit: mm
1398.2 Max
1242.8
1087.5
932.11
776.75
621.4
466.05
310.7
155.35
0 Min
Max
Z
Y
X

Chapter 6 Variability analysis of pinna deformation

Principal Component Analysis (PCA) serves as a powerful statistical technique applied in various fields, including engineering and computational modeling. In the context of structural analysis using ANSYS, PCA is employed to discern the minimum possible number of eigenvalue and eigenvector combinations necessary to adequately describe the set of deformation data gathered from the simulation.

The primary objective of PCA is to reduce the dimensionality of complex datasets while retaining the essential information. In the case of ANSYS simulation results, PCA becomes instrumental in identifying the principal components or modes that contribute significantly to the observed deformation patterns. By extracting these principal components, which are essentially linear combinations of the original deformation variables, PCA enables a more concise representation of the data.

The concept of eigenvalues and eigenvectors plays a pivotal role in PCA. Eigenvalues signify the amount of variance explained by each principal component, while eigenvectors denote the direction of maximum variance in the dataset. Through PCA, one can systematically determine which modes capture the most substantial variability in the deformation data.

Moreover, by selecting only the principal components that account for the majority of the variance, PCA facilitates a more efficient representation of the structural response. This reduction in dimensionality not only aids in simplifying the interpretation of results but also contributes to computational efficiency.

In summary, PCA applied to the deformation data obtained from ANSYS simulations is a methodical approach to distilling the essential patterns and characteristics of structural behavior. It involves determining the minimum set of eigenvalues and eigenvectors that effectively capture the underlying variability in the dataset, providing valuable insights for further analysis and interpretation.

In the presented figure 30, a comparative analysis is conducted on the number of eigenvalues between two scenarios: nonparallel and parallel computations. Notably, the examination reveals a distinct advantage in the parallel approach, where a reduced number of eigenvalues is necessary compared to the nonparallel counterpart. Specifically, the count for the parallel computation, denoted as N parallel, stands at 5, while the nonparallel computation requires a larger set, denoted as N nonparallel, with a count of 7. The code will be in appendix C.

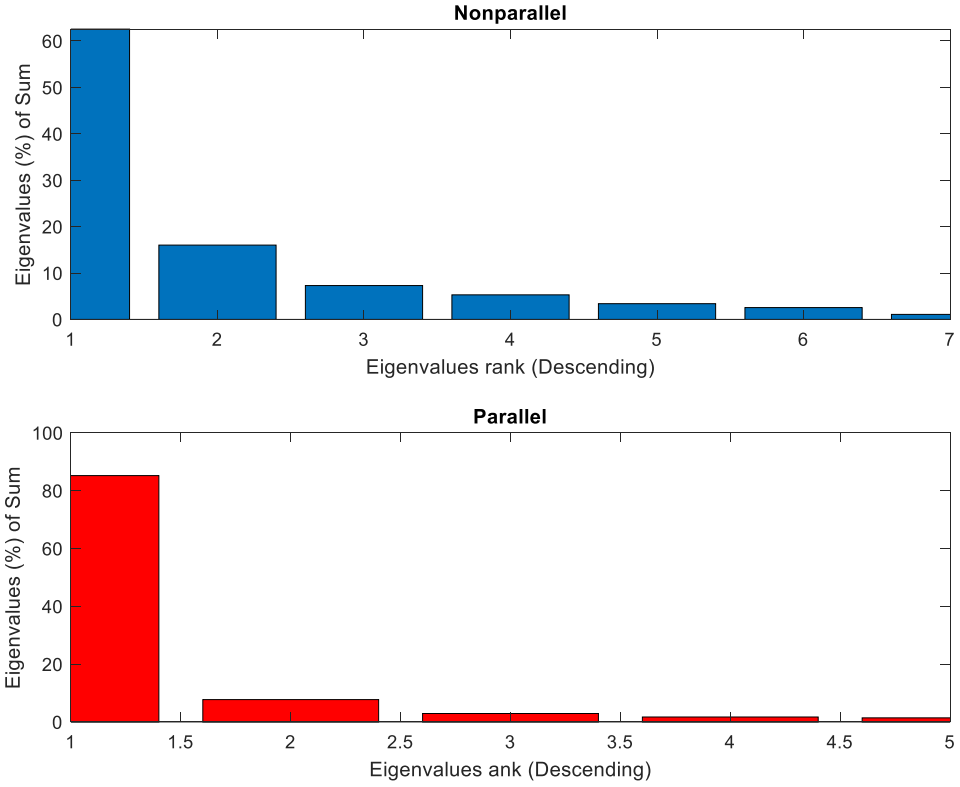

Figure 30: Eigenvalues for parallel and nonparallel.

This discrepancy in the required number of eigenvalues suggests that the parallel computation methodology achieves its results or desired outcomes with greater efficiency, necessitating fewer computational steps than its nonparallel counterpart. Such efficiency gains in the parallel approach can have significant implications for computational performance and resource utilization. Further exploration into the underlying algorithms and methodologies employed in both scenarios could provide valuable insights into the mechanisms contributing to this observed difference. Understanding these nuances may be crucial for optimizing computational processes and improving overall efficiency in related applications.

In the provided figure 31, an examination of the absolute values of eigenvalues for both nonparallel and parallel configurations is depicted. Notably, the plot illustrates that the eigenvalues in the parallel scenario exhibit higher magnitudes compared to their nonparallel counterparts. This discrepancy in magnitude provides a key insight into the observed phenomenon where a lesser number of eigenvalues are required in the parallel case.

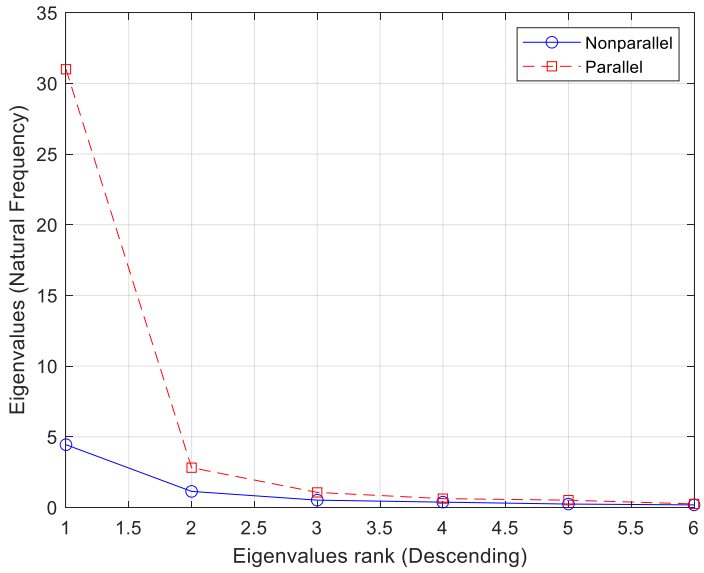

Figure 31: Absolute values of eigenvalues.

The higher absolute values of parallel eigenvalues suggest that a more substantial amount of modal information is encapsulated in each eigenvalue and its corresponding eigenvector pair. This phenomenon implies that parallel computation can capture and represent essential system dynamics with fewer eigenvalues, streamlining the storage of modal information.

Understanding this distinction in eigenvalue magnitudes sheds light on the efficiency gains observed in the parallel approach. The ability to encapsulate more modal information within individual eigenvalues can lead to a more concise representation of the system's behavior, ultimately contributing to the reduced need for a larger set of eigenvalues in comparison to the nonparallel configuration.

Further analysis and exploration of the specific characteristics of the eigenvalue-eigenvector pairs in both scenarios can provide valuable insights into the underlying mechanisms contributing to this observed behavior. Such insights are crucial for refining computational strategies, optimizing resource utilization, and enhancing the overall efficiency of applications relying on eigenvalue analysis.

In the depicted figure 32, the deformation of both nonparallel and parallel configurations is presented, facilitating a direct comparison to elucidate the impact of each mesh structure on the absolute values. This visual representation serves to discern and analyze how the chosen mesh configurations influence the magnitude of deformation in the studied system.

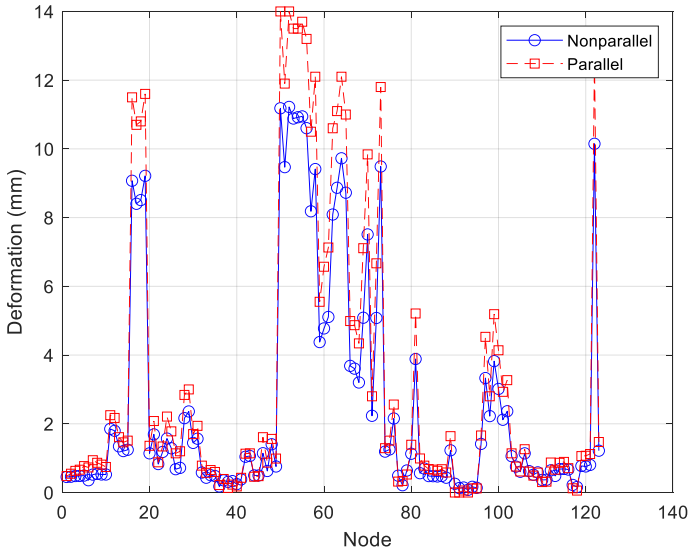

Figure 32: Absolute deformation.

The comparison between the nonparallel and parallel deformations provides valuable insights into the structural response under the distinct mesh arrangements. Variations in the absolute values of deformation observed in the figure can offer an understanding of how each mesh structure contributes to the overall behavior of the system.

Analyzing and interpreting these deformation patterns is crucial for gaining insights into the mechanical characteristics of the system under different mesh configurations. Such comparative studies are fundamental in engineering and scientific analyses, as they contribute to optimizing mesh designs, refining simulation methodologies, and enhancing the accuracy of predictive models.

Further investigation into the specific features of the deformations, as highlighted in the figure, can yield a deeper understanding of the system's response to different mesh structures. This knowledge is instrumental in refining and tailoring computational

models to represent real-world scenarios more accurately, ultimately contributing to advancements in simulation accuracy and reliability.

Table 15 shows the Second moment (Standard Deviation) for and the Third moment (Skewness) both parallel, and nonparallel.

Table 15: Second and third moments

	Parallel	Nonparallel
Second Moment (Standard Deviation)	2.4653	6.5461
Third Moment (Skewness)	10.7977	9.7827

The second moment for the nonparallel configuration was presented as a cost function for utilization in the genetic algorithm.

Chapter 7 Optimization of the actuation patterns

This chapter explores the optimization of a robust design for a 5-actuator pinna utilizing the genetic algorithm (GA). The GA is employed to enhance fitness function, starting with the initialization of a population featuring randomly assigned parameter values. The fitness of each individual within the population is then evaluated. Subsequent operations, including selection, crossover, and mutation, contribute to the generation of a new population based on selected parents and mutated offspring. This iterative process spans multiple generations, and the evolving fitness values are plotted over time. The ultimate goal of GA optimization is to identify optimal parameters for the robust design, including the x and y positions, angle, and length of each actuator. The detailed code, available in Appendix D, outlines the initialization, population generation, and the iterative optimization loop. Figure 33 presents a plot illustrating the evolution of maximum and average fitness over 15 generations, with fitness measured as the percentage normalization of the eigenvalue. The termination criteria include a population size of 15 and a mutation probability of 0.1. In summary, the GA efficiently explores complex solution spaces, proving to be a valuable tool for addressing optimization challenges in diverse domains. Its ongoing refinement ensures its continued relevance and advancement.

Code Implementation Overview:

The provided code is not sourced from a library; instead, it represents a basic implementation of a genetic algorithm (GA). The key steps include:

Generating an initial population with random parameter values and verifying the feasibility of the pinna configuration.

Iterating over generations:

a. Performing crossover between two parents, checking feasibility and fitness, and adding feasible offspring to the population.

b. Implementing mutation by randomly selecting individuals from the population, randomly altering a gene, and verifying feasibility and fitness before adding the mutated offspring to the population.

c. Sorting the population based on fitness and discarding the least fit individuals to maintain a consistent population size across generations.

d. Saving the results.

Generating a plot to visualize the evolution of fitness over generations.

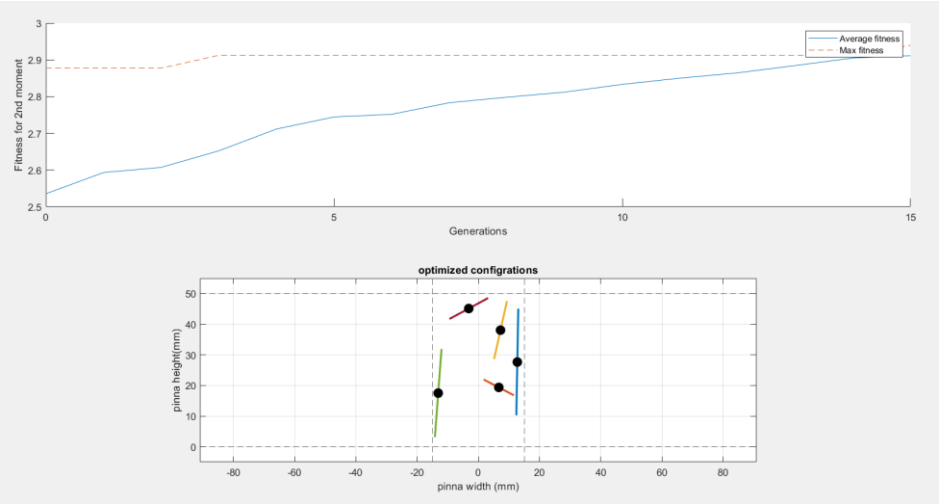

Figure 33: Optimized configuration.

Figure 34 shows the optimized configurations among all the other offspring's and selects the best individual from the population and displays the actuators' configuration in 3D.

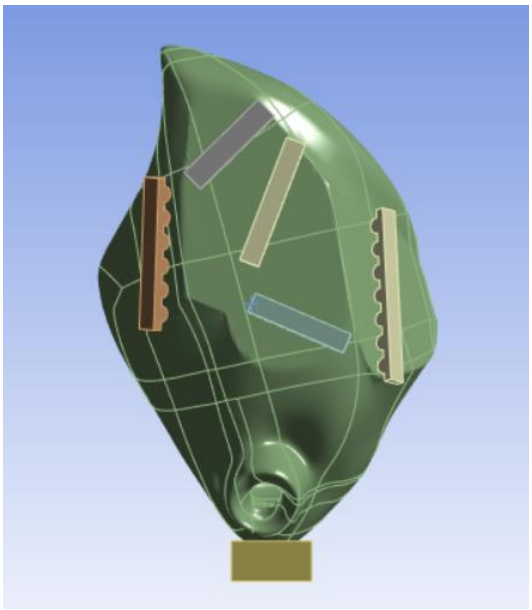

Figure 34: Optimized 3D configuration.

Following the implementation of the 3D shape on Ansys, replicate the entire process for the parametric study. Begin by assigning identical mesh size, material, boundary conditions, and loads for the 243 combinations derived from the activation pattern (0, 1.5, and 3) N. Figure 35 illustrates 8 examples (12.941, 48.489, 29.136, 31.889, 17.516, 20.866,43.656, and 3.8921e^-5) mm of optimized 3D configurations out of the 243; the remaining results are available in the appendix.

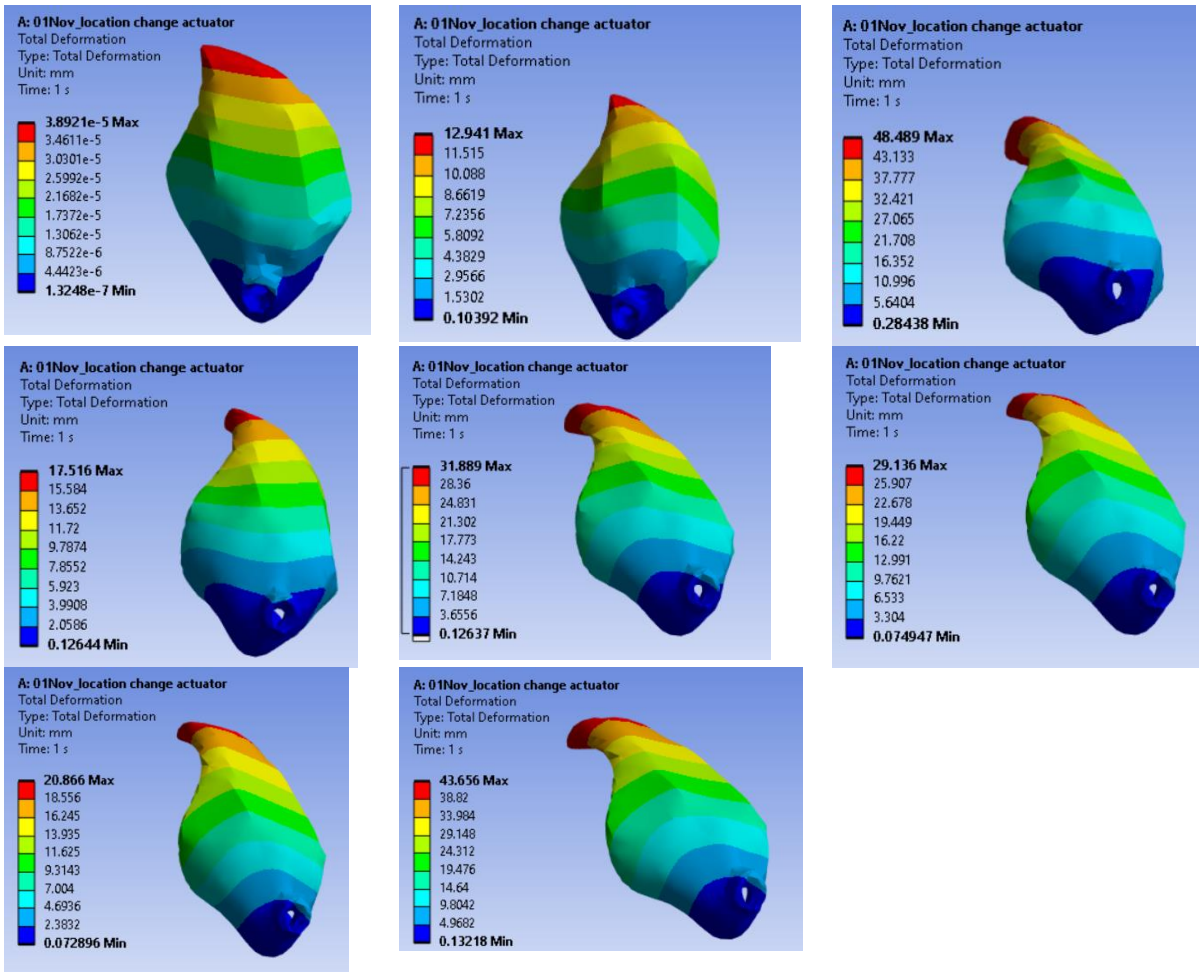

Figure 35: Optimized results for nonparallel. (See Appendix L)

Figure 36 showcases the eigenvalues obtained for optimized nonparallel results after applying the genetic algorithm. Initially requiring 7 eigenvalues, the current configuration now only requires 5 eigenvalues. This indicates that the process stops when the cumulative sum exceeds 99%, and no more eigenvalues are included. In simpler terms, the focus is on eigenvalues less than 1%.

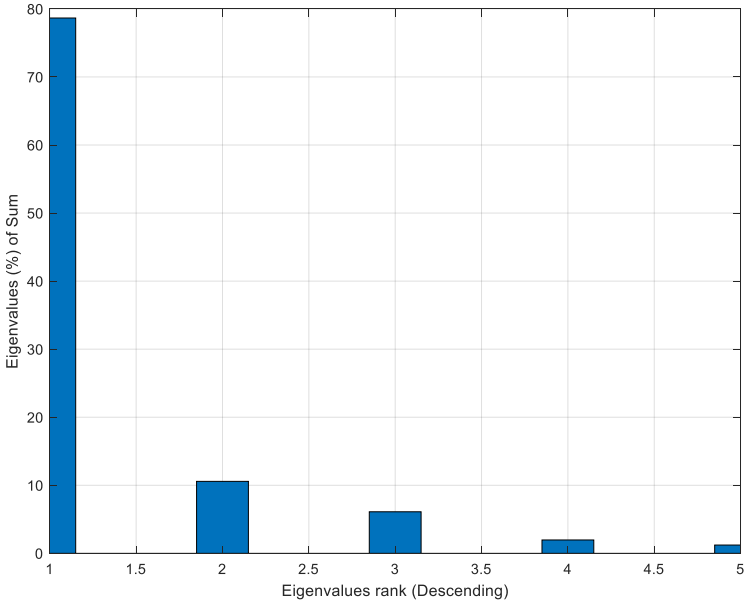

Figure 36: Eigenvalues for optimized nonparallel.

Figure 37 depicts the absolute values of the eigenvalues for the optimized nonparallel configuration. The examination focuses on the absolute values of eigenvalues in the optimized nonparallel configuration, revealing a significant difference as the plot demonstrates higher magnitudes in the optimized nonparallel scenario compared to their nonparallel counterparts. This discrepancy implies that the optimized nonparallel computation captures and represents essential system dynamics more efficiently,

requiring fewer eigenvalues. The elevated absolute values in the optimized nonparallel eigenvalues suggest a more comprehensive encapsulation of modal information in each eigenvalue and its corresponding eigenvector pair, streamlining the storage of modal information. This efficiency gain is crucial, reducing the necessity for a larger set of eigenvalues in comparison to the nonparallel configuration. Further exploration into the specific characteristics of the eigenvalue-eigenvector pairs in both scenarios promises valuable insights into the underlying mechanisms, offering opportunities for refining computational strategies and enhancing the overall efficiency of applications relying on eigenvalue analysis.

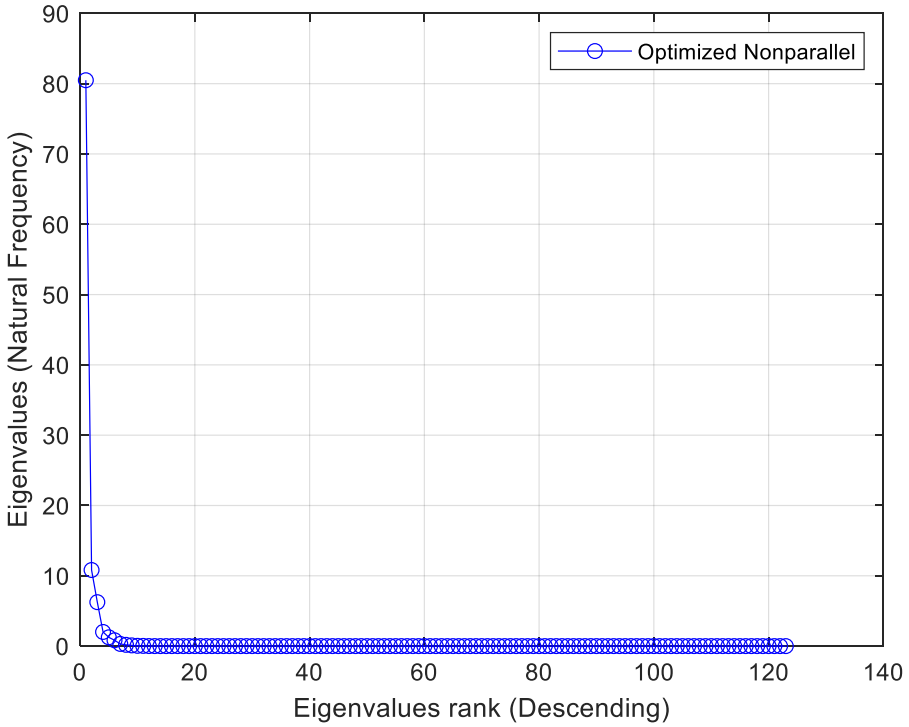

Figure 37: Absolute values of eigenvalues.

Figure 38 illustrates a direct comparison, allowing for a clear understanding of the influence of each mesh structure on absolute values. This visual representation aids in discerning and analyzing the impact of selected mesh configurations on the magnitude of deformation within the studied system.

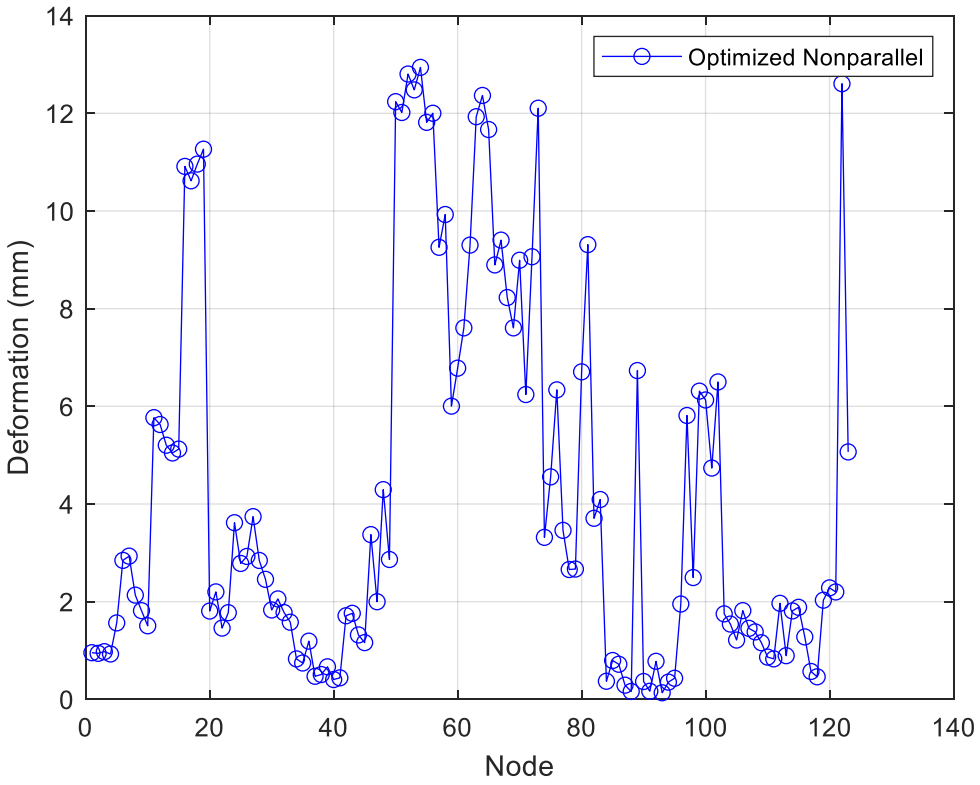

Figure 38: Absolute deformation.

Chapter 8 Acoustics

Harmonic acoustics is a branch of acoustics that focuses on the mathematical analysis and understanding of sound waves, particularly in the context of harmonic structures. In the realm of physics and mathematics, harmonics refer to the overtones or multiples of the fundamental frequency of a sound wave. The study of harmonic acoustics involves examining how these harmonic components contribute to the overall characteristics of a sound signal.

Key concepts within harmonic acoustics include:

Fundamental Frequency: The lowest frequency component of a sound wave, often corresponding to the perceived pitch of a musical note. In harmonic acoustics, the fundamental frequency serves as the base upon which harmonics are built.

Harmonics: These are multiples of the fundamental frequency and are responsible for shaping the timbre or quality of a sound. In musical instruments, the presence and relative amplitudes of harmonics contribute to the instrument's unique sound.

Overtone Series: The overtone series represents the sequence of harmonics present in a sound wave. Each harmonic has a specific frequency and amplitude, and the combination of these harmonics determines the overall sound character.

Fourier Analysis: A mathematical tool used in harmonic acoustics to decompose complex waveforms into their constituent frequencies. Fourier analysis helps in understanding the spectral content of a sound signal, revealing the contribution of individual harmonics.

Resonance: Harmonic acoustics often explores resonance phenomena, where certain frequencies are amplified due to the natural frequency characteristics of a medium or an object. Resonance plays a crucial role in the behavior of musical instruments and in the transmission of sound waves through various materials.

Harmonic Content in Musical Instruments: Different musical instruments produce unique harmonic signatures. The study of harmonic acoustics helps explain why instruments such as guitars, pianos, and violins have distinct sounds and how their construction influences the harmonic content.

Psychoacoustics: Understanding how the human ear perceives and processes harmonic content is another aspect of harmonic acoustics. Psychoacoustic principles help explain why certain harmonic structures are more pleasing or distinguishable to the human ear.

In summary, harmonic acoustics provides a systematic and mathematical framework for analyzing and understanding the complex interplay of frequencies that make up sound waves. This knowledge is crucial not only in the design and construction of musical instruments but also in various applications such as audio engineering, acoustical design, and the study of sound perception.

Patch Conforming Method:

This is likely a meshing technique that conforms to the geometry of specific components like the air boundary, pinna, actuators, and other parts. It's a common approach in FEA and CFD to generate meshes that accurately represent the geometry of the objects being analyzed.

Body Sizing as shown in figure 39:

Refers to the mesh size assigned to different components.

5mm body sizing is used for the air boundary.

2mm body sizing is used for the pinna.

3mm body sizing is used for actuators.

2mm body sizing is used for other parts.

Body sizing determines the resolution of the mesh and is often chosen based on the features or importance of each component in the analysis.

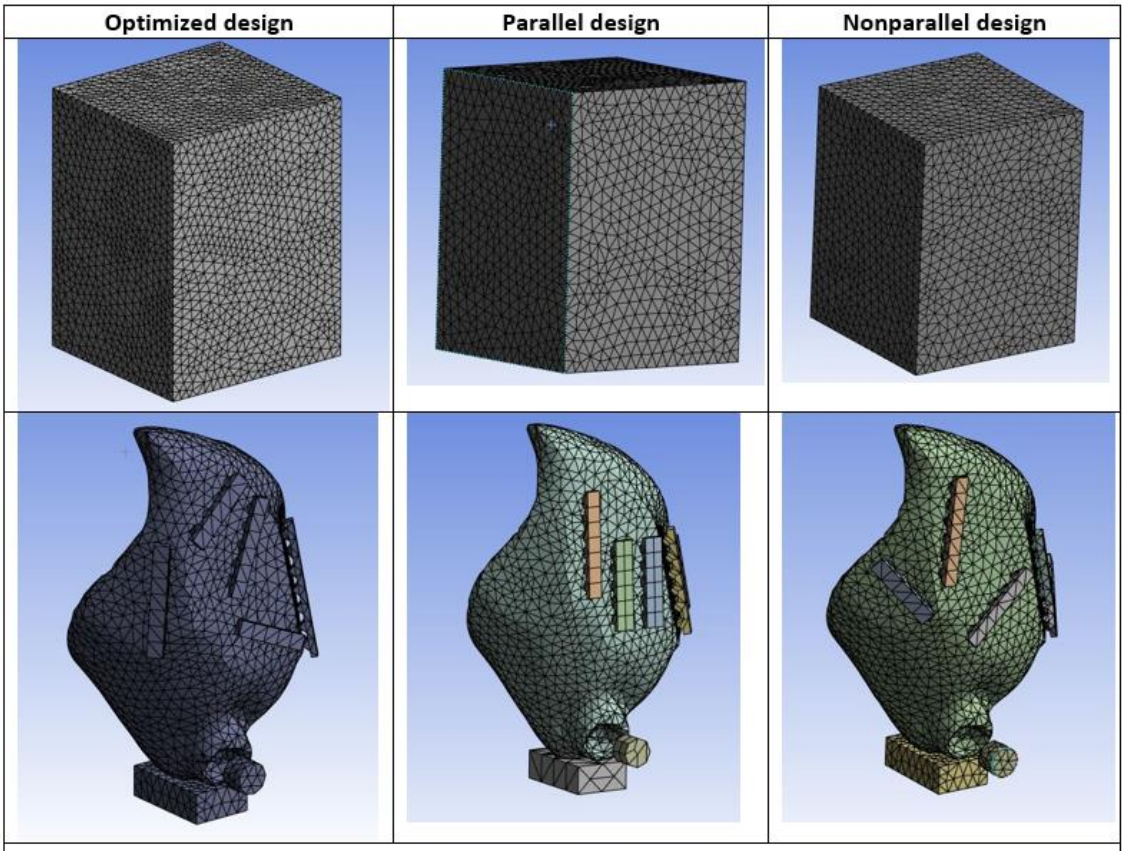

Figure 39: Meshing methodology

Mesh Step Sequence:

Describes the order in which different components are meshed.

Step 1: Mesh the air boundary using a 5mm body size.

Step 2: Mesh the actuators using a 3mm body size.

Step 3: Mesh the pinna using a 2mm body size.

Step 4: Mesh other parts using a 2mm body size.

Following a specific sequence may be essential for maintaining the overall integrity of the mesh and ensuring compatibility between different components. In ANSYS Acoustics, modeling an outer enclosure as an acoustic region is essential for accurate acoustic analysis. The outer enclosure serves as a boundary condition that defines the limits of the computational domain and influences the acoustic behavior of the system. When setting up an outer enclosure, the various boundary conditions to accurately simulate the acoustic environment.

Pipe as a mass source

The pipe would be acting as a mass source of 0.1 kg/s. In ANSYS Acoustics, a mass source boundary condition is used to model the introduction of acoustic energy into the

computational domain. This condition represents a localized region where acoustic waves are generated, typically by an external source like a speaker or vibrating surface.

Pinna as a physical body

The pinna geometry would be acting as a physical body. The, effect of acoustics were studied such as deformation on the physical body of pinna. as shown in figure 40.

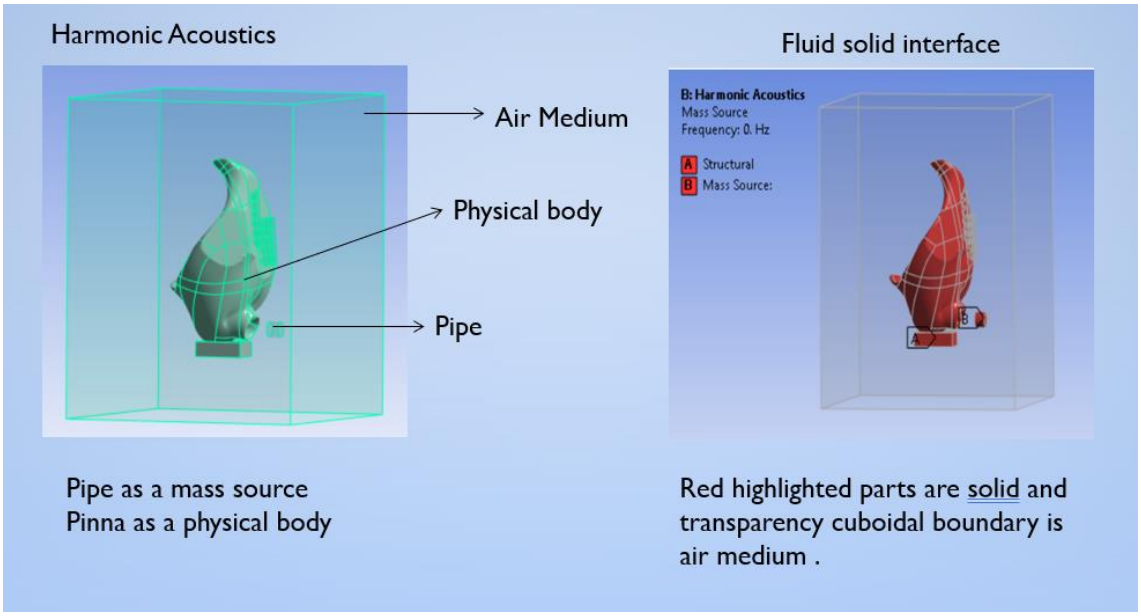

Figure 40: Overall integrity of the mesh

Reasoning:

Shared topology and space claim for acoustic requirements suggest that the components are interconnected or affect each other acoustically.

The use of different body sizing for different components reflects the importance of capturing fine details in certain areas (e.g., pinna) and optimizing computational resources in others (e.g., air boundary). Fluid solid interface

When dealing with a fluid-solid interaction, boundaries where fluid and solid regions come into contact are represented by this interface. Properly defining the boundary conditions at these interfaces is crucial for accurate simulations. Radiation boundary on surfaces of enclosure A radiation boundary condition on the surfaces of an enclosure in ANSYS Acoustics is used to model the transmission or absorption of acoustic waves through these surfaces. This condition allows sound waves to leave the computational domain without reflecting back.as shown in figure 41.

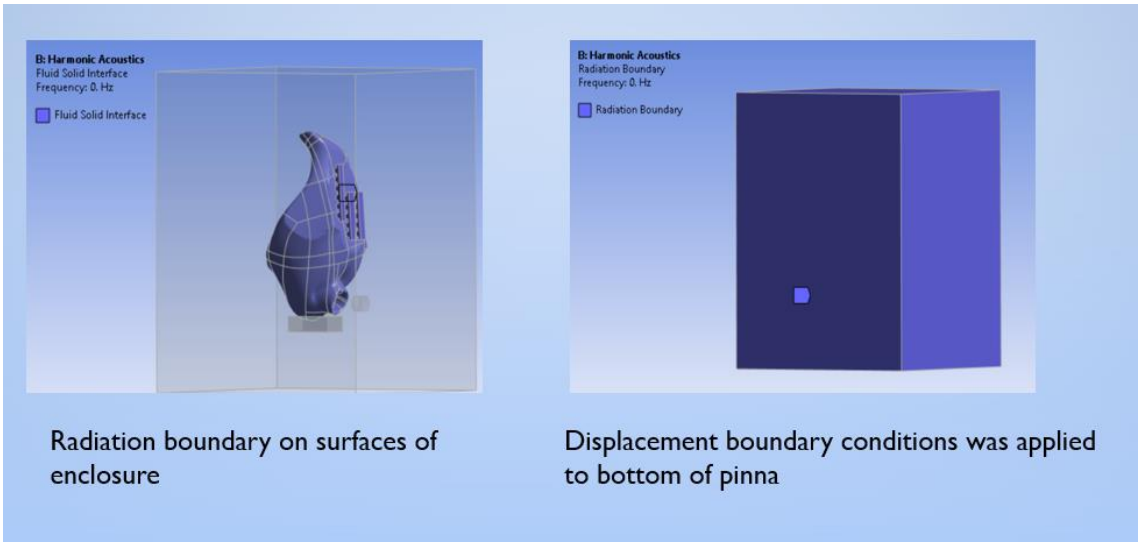

Figure 41: Boundary conditions

Conforming the mesh to the geometry is crucial for accurate simulations, especially in acoustics where small features can have a significant impact.

In summary, it appears that the described method is a systematic approach to meshing different components with specific considerations for body sizing and sequence. This

process is likely tailored to the acoustic simulation requirements, ensuring a balance between accuracy and computational efficiency.

Displacement boundary conditions was applied to bottom of pinna

In ANSYS Acoustics, displacement boundary conditions are applied to model the structural response of a system to acoustic loads. These conditions are used to restrict the movement or deformation of structural surfaces or nodes. The bottom surface of the pinna was applied with displacement boundary conditions.

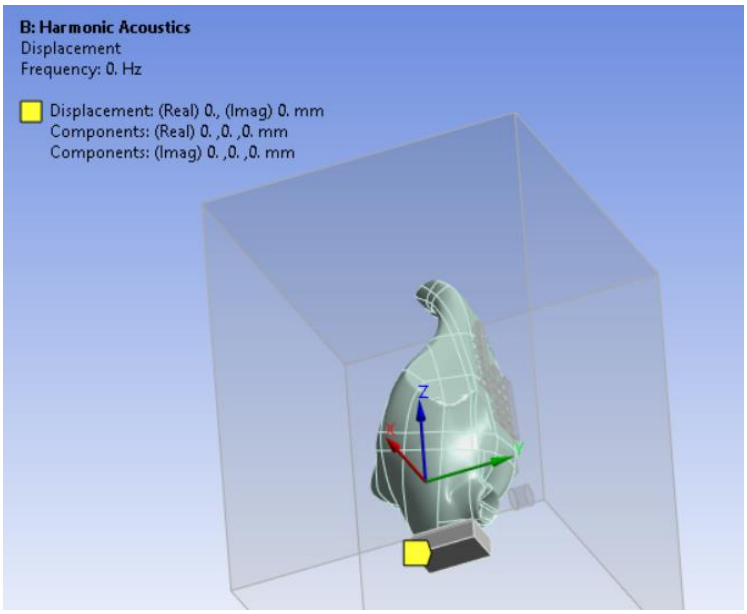

Figure 42: displacement boundary conditions.

Nonparallel and Parallel Deformation at Pinna:

The description suggests that the maximum deformation is found at the same location in both the nonparallel and parallel models. However, there is only a slight difference in the variation of values at a specific frequency, 5000Hz.This implies that, in general, the deformation patterns are similar, but there is a subtle discrepancy in the magnitude of deformation at this particular frequency.

Optimized design:

In the optimized model, the maximum deformation is found at the top location of the pinna. This is a deviation from the nonparallel and parallel models, where the maximum deformation was found at the same location as shown in figure 43.

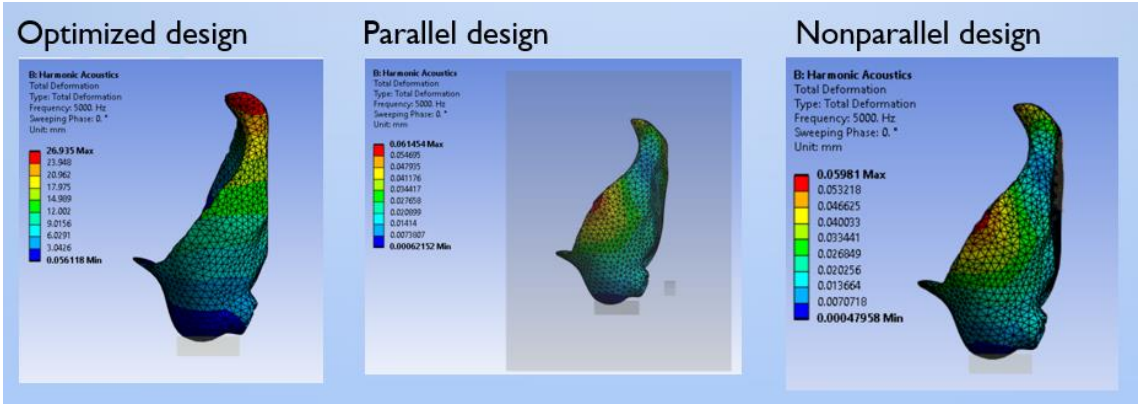

Figure 43: Acoustic results

Frequency Variation (5000Hz):

The mention of a specific frequency, 5000Hz, indicates that the analysis is focusing on the harmonic content of the acoustics, as frequencies in this range are often associated with mid-range frequencies in human hearing.

Implications:

The fact that the optimized model shows a different location for maximum deformation may suggest that certain design or optimization changes have influenced the structural response of the pinna at specific frequencies. The slight difference in deformation values at 5000Hz in the nonparallel and parallel models could be attributed to variations in the geometry or material properties considered in each scenario.

Considerations:

Further analysis may be needed to understand why the optimized model exhibits a different deformation pattern and whether this change aligns with the intended design goals. It's essential to consider the potential impact of these deformation patterns on the acoustics, especially in terms of how they may affect sound localization, amplification, or attenuation.

In conclusion, the information you provided suggests a nuanced understanding of deformation patterns in the pinna across different scenarios, with a specific focus on the influence of frequency content. Analyzing the differences in deformation patterns can provide valuable insights into the structural behavior of the pinna in the context of harmonic acoustics.

Chapter 9 Conclusion and recommendations for future work

9.1 Conclusion

In conclusion, bats are renowned for their remarkable biosonar systems, facilitating agile movement and precise hunting within dense foliage. Their biosonar mechanism comprises a single emitter (mouth or nose) and two receivers (ears). Certain bat species exhibit intricate pinna motion patterns, classified into stiff and non-rigid movements. This thesis explored the mechanics of pinna sensing, elucidating diverse rotation and curvature patterns within rigid and non-stiffened pinnae.

The research journey began with a comprehensive exploration of design concepts, unveiling the intricate interplay between actuator geometry and resultant pinna deformation. A systematic optimization process employed tiered forces, and Finite Element Analysis (FEA) simulations were bolstered by material characterization for accurate deformation quantification. Principal Component Analysis (PCA) further uncovered variability among deformation patterns.

The pinnacle of the study featured the application of Genetic Algorithms (GA), enabling fine-tuning of deformation for pronounced pinna variability. The sequential trajectory encompassed design conceptualization, force-driven optimization, FEA simulations

with material characterization, PCA-based variability analysis, and GA-enabled morphological diversity induction.

This work strategically progressed through design concept exploration, force-induced optimization, FEA simulations with material considerations, PCA-based variability analysis, and culminated in GA-assisted pinna configuration diversification. By employing design code, applying varied forces, conducting simulations, and leveraging optimization algorithms, the research attained its primary objective of achieving substantial pinna shape variability.

In summary, this study provided a comprehensive journey starting from design exploration, optimization through forces, simulations with FEA and material characterization, PCA variability analysis, and finally GA-aided shape diversity attainment. This thorough investigation deepened our understanding of pinna mechanics and holds the potential to inspire advancements in bio-inspired design and engineering.

9.2 Recommendations for future work

Building on the insights gained from the current study, several avenues for future research and development emerge:

- Multi-Actuator Interaction: Investigate the interactions among multiple actuators to determine if complex coordinated movements can be achieved.

This could lead to more sophisticated pinna deformation patterns that closely mimic natural bat pinna motions.

- Dynamic Simulation: Extend the analysis to dynamic scenarios, simulating real-time pinna responses during bat flight or motion. This would provide a more comprehensive understanding of how pinnae adapt to varying external conditions.

- Experimental Validation: Conduct experimental tests to validate the simulated results. Construct physical prototypes with actuators to verify the predicted deformation patterns and compare them with the simulated outcomes.

- Variable Material Properties: Introduce variable material properties within the pinna structure to mimic the heterogeneous nature of biological tissues. This could provide a more accurate representation of pinna behavior under different loading conditions.

- Optimization Beyond GA: Explore advanced optimization techniques beyond Genetic Algorithms, such as particle swarm optimization, to further refine the pinna deformation patterns and enhance the diversity achieved.

- Real-time Adaptation: Develop adaptive control strategies that allow the actuators to respond in real time to changing environments or acoustic conditions. This could lead to more efficient and effective biosonar-inspired systems.

- Acoustic Performance Analysis: Extend the analysis to investigate how the achieved pinna configurations impact the acoustic properties of the biosonar system. Assess the directional sensitivity and frequency response of the system in various environments.

- Integration with Robotic Systems: Implement the optimized pinna deformation patterns on robotic systems equipped with biosonar capabilities. This could lead to the development of more advanced and agile robotic platforms for tasks such as environmental exploration and navigation.

- Bio-Inspired Applications: Explore broader applications of the pinna deformation principles in fields beyond biosonar, such as adaptive structures, aerospace engineering, and medical devices.

- Human-AI Collaboration: Investigate the synergy between human intuition and AI-driven optimization. Develop interfaces that allow engineers and designers to collaborate with AI algorithms in refining pinna designs.

- Ethological Studies: Collaborate with biologists to gain deeper insights into the biomechanics of bat pinna motion in various ecological contexts. This could help refine the design criteria and inspire more accurate simulations.

- Miniaturization and Efficiency: Explore ways to miniaturize the actuators and optimize their energy efficiency, enabling the creation of compact and energy-efficient bio-inspired systems.

- By embarking on these future directions, the research can continue to contribute to the fields of bio-inspired engineering, robotics, and acoustic technology, ultimately pushing the boundaries of our understanding and capabilities in mimicking nature for innovative design solutions.

References

Apsite, I., Salehi, S., & Ionov, L. (2022). Materials for Smart Soft Actuator Systems. *Chemical Reviews*, *122*(1), 1349–1415. https://doi.org/10.1021/acs.chemrev.1c00453

Argentieri, S., Danès, P., & Souères, P. (2015). A survey on sound source localization in robotics: From binaural to array processing methods. *Computer Speech & Language*, *34*(1), 87–112. https://doi.org/10.1016/j.csl.2015.03.003

Argentieri, S., Portello, A., Bernard, M., Danès, P., & Gas, B. (2013). Binaural Systems in Robotics. In *The Technology of Binaural Listening* (pp. 225–253). Springer Berlin Heidelberg. https://doi.org/10.1007/978-3-642-37762-4_9

Bailey, W. J. (1993). The tettigoniid (Orthoptera : Tettigoniidae) ear: Multiple functions and structural diversity. *International Journal of Insect Morphology and Embryology*, *22*(2–4), 185–205. https://doi.org/10.1016/0020-7322(93)90009-P

Bar-Cohen, Y. (2011). Biological Senses as Inspiring Model for Biomimetic Sensors. *IEEE Sensors Journal*, *11*(12), 3194–3201. https://doi.org/10.1109/JSEN.2011.2167321

Bhamare, N., Tardalkar, K., Khadilkar, A., Parulekar, P., & Joshi, M. G. (2022). Tissue engineering of human ear pinna. *Cell and Tissue Banking*, *23*(3), 441–457. https://doi.org/10.1007/s10561-022-09991-7

Bhandari, P. S. (1998). Total ear reconstruction in post burn deformity. *Burns*, *24*(7), 661–670. https://doi.org/10.1016/S0305-4179(98)00093-X

Boonman, A., Bumrungsri, S., & Yovel, Y. (2014). Nonecholocating Fruit Bats Produce Biosonar Clicks with Their Wings. *Current Biology*, *24*(24), 2962–2967. https://doi.org/10.1016/j.cub.2014.10.077

Burdick, J. A., & Prestwich, G. D. (2011). Hyaluronic Acid Hydrogels for Biomedical Applications. *Advanced Materials*, *23*(12), H41–H56. https://doi.org/10.1002/adma.201003963

Buytaert, J. A. N., Salih, W. H. M., Dierick, M., Jacobs, P., & Dirckx, J. J. J. (2011). Realistic 3D Computer Model of the Gerbil Middle Ear, Featuring Accurate Morphology of Bone and Soft Tissue Structures. *Journal of the Association for Research in Otolaryngology*, *12*(6), 681–696. https://doi.org/10.1007/s10162-011-0281-4

Byrne, D., & Noble, W. (1998). Optimizing Sound Localization with Hearing Aids. *Trends in Amplification*, *3*(2), 51–73. https://doi.org/10.1177/108471389800300202

Chen Austin, M., Garzola, D., Delgado, N., Jiménez, J. U., & Mora, D. (2020). Inspection of Biomimicry Approaches as an Alternative to Address Climate-Related Energy Building

Challenges: A Framework for Application in Panama. *Biomimetics*, *5*(3), 40. https://doi.org/10.3390/biomimetics5030040

Chiang-Jung Pu, Harris, J. G., & Principe, J. C. (1997). A neuromorphic microphone for sound localization. *1997 IEEE International Conference on Systems, Man, and Cybernetics. Computational Cybernetics and Simulation*, 1469–1474. https://doi.org/10.1109/ICSMC.1997.638190

Chung, J. H. Y., Kade, J., Jeiranikhameneh, A., Yue, Z., Mukherjee, P., & Wallace, G. G. (2018). A bioprinting printing approach to regenerate cartilage for microtia treatment. *Bioprinting*, *12*, e00031. https://doi.org/10.1016/j.bprint.2018.e00031

Corni, I., Harvey, T. J., Wharton, J. A., Stokes, K. R., Walsh, F. C., & Wood, R. J. K. (2012). A review of experimental techniques to produce a nacre-like structure. *Bioinspiration & Biomimetics*, *7*(3), 031001. https://doi.org/10.1088/1748-3182/7/3/031001

Fenton, B., Jensen, F. H., Kalko, E. K. V., & Tyack, P. L. (2014). *Sonar Signals of Bats and Toothed Whales* (pp. 11–59). https://doi.org/10.1007/978-1-4614-9146-0_2

Fu, S., Wei, F., Yin, C., Yao, L., & Wang, Y. (2021). Biomimetic soft micro-swimmers: from actuation mechanisms to applications. *Biomedical Microdevices*, *23*(1), 6. https://doi.org/10.1007/s10544-021-00546-3

Fujioka, E., Fukushiro, M., Ushio, K., Kohyama, K., Habe, H., & Hiryu, S. (2021). Three-Dimensional Trajectory Construction and Observation of Group Behavior of Wild Bats During Cave Emergence. *Journal of Robotics and Mechatronics*, *33*(3), 556–563. https://doi.org/10.20965/jrm.2021.p0556

Heidemann, J., Wei Ye, Wills, J., Syed, A., & Yuan Li. (2006). Research challenges and applications for underwater sensor networking. *IEEE Wireless Communications and Networking Conference, 2006. WCNC 2006.*, 228–235. https://doi.org/10.1109/WCNC.2006.1683469

Hiraga, T., Yamada, Y., & Kobayashi, R. (2022). Theoretical investigation of active listening behavior based on the echolocation of CF-FM bats. *PLOS Computational Biology*, *18*(10), e1009784. https://doi.org/10.1371/journal.pcbi.1009784

Jung, Y. H., Park, B., Kim, J. U., & Kim, T. (2019). Bioinspired Electronics for Artificial Sensory Systems. *Advanced Materials*, *31*(34), 1803637. https://doi.org/10.1002/adma.201803637

Kim, U.-H., & Okuno, H. G. (2013). Improved binaural sound localization and tracking for unknown time-varying number of speakers. *Advanced Robotics*, *27*(15), 1161–1173. https://doi.org/10.1080/01691864.2013.812177

Lee, H. S., Chung, J., Hwang, G.-T., Jeong, C. K., Jung, Y., Kwak, J.-H., Kang, H., Byun, M., Kim, W. D., Hur, S., Oh, S.-H., & Lee, K. J. (2014). Flexible Inorganic Piezoelectric Acoustic Nanosensors for Biomimetic Artificial Hair Cells. *Advanced Functional Materials*, *24*(44), 6914–6921. https://doi.org/10.1002/adfm.201402270

Li, H., Sinha, T. K., Oh, J. S., & Kim, J. K. (2018). Soft and Flexible Bilayer Thermoplastic Polyurethane Foam for Development of Bioinspired Artificial Skin. *ACS Applied Materials & Interfaces*, *10*(16), 14008–14016. https://doi.org/10.1021/acsami.8b01026

Liu, Z., Zhang, Z., & Ritchie, R. O. (2020). Structural Orientation and Anisotropy in Biological Materials: Functional Designs and Mechanics. *Advanced Functional Materials*, *30*(10), 1908121. https://doi.org/10.1002/adfm.201908121

Müller, R. (2015). Dynamics of biosonar systems in Horseshoe bats. *The European Physical Journal Special Topics*, *224*(17–18), 3393–3406. https://doi.org/10.1140/epjst/e2015-50089-7

Müller, R., Abaid, N., Boreyko, J. B., Fowlkes, C., Goel, A. K., Grimm, C., Jung, S., Kennedy, B., Murphy, C., Cushing, N. D., & Han, J.-P. (2018). Biodiversifying bioinspiration. *Bioinspiration & Biomimetics*, *13*(5), 053001. https://doi.org/10.1088/1748-3190/aac96a

Müller, R., & Kuc, R. (2007). Biosonar-inspired technology: goals, challenges and insights. *Bioinspiration & Biomimetics*, *2*(4), S146–S161. https://doi.org/10.1088/1748-3182/2/4/S04

Müller, R., Pannala, M., Praveen K Reddy, O., & Meymand, S. Z. (2012). Design of a dynamic sensor inspired by bat ears. *Smart Materials and Structures*, *21*(9), 094025. https://doi.org/10.1088/0964-1726/21/9/094025

Nothwang, H. G. (2016). Evolution of mammalian sound localization circuits: A developmental perspective. *Progress in Neurobiology*, *141*, 1–24. https://doi.org/10.1016/j.pneurobio.2016.02.003

Okoro, C. K., Kingsley, R. A., Connor, T. R., Harris, S. R., Parry, C. M., Al-Mashhadani, M. N., Kariuki, S., Msefula, C. L., Gordon, M. A., de Pinna, E., Wain, J., Heyderman, R. S., Obaro, S., Alonso, P. L., Mandomando, I., MacLennan, C. A., Tapia, M. D., Levine, M. M., Tennant, S. M., … Dougan, G. (2012). Intracontinental spread of human invasive Salmonella Typhimurium pathovariants in sub-Saharan Africa. *Nature Genetics*, *44*(11), 1215–1221. https://doi.org/10.1038/ng.2423

Pedersen, S. C., & Müller, R. (2013). Nasal-Emission and Nose leaves. In *Bat Evolution, Ecology, and Conservation* (pp. 71–91). Springer New York. https://doi.org/10.1007/978-1-4614-7397-8_4

Peremans, H., & Reijniers, J. (2005). *The CIRCE Head: A Biomimetic Sonar System* (pp. 283–288). https://doi.org/10.1007/11550822_45

Pulver, C. A., Celiker, E., Woodrow, C., Geipel, I., Soulsbury, C. D., Cullen, D. A., Rogers, S. M., Veitch, D., & Montealegre-Z, F. (2022). Ear pinnae in a neotropical katydid (Orthoptera: Tettigoniidae) function as ultrasound guides for bat detection. *ELife*, *11*. https://doi.org/10.7554/eLife.77628

Rabbitt, R. D., & Holmes, M. H. (1988). Three-dimensional acoustic waves in the ear canal and their interaction with the tympanic membrane. *The Journal of the Acoustical Society of America*, *83*(3), 1064–1080. https://doi.org/10.1121/1.396051

Ren, J., Wang, Y., Yao, Y., Wang, Y., Fei, X., Qi, P., Lin, S., Kaplan, D. L., Buehler, M. J., & Ling, S. (2019). Biological Material Interfaces as Inspiration for Mechanical and Optical Material Designs. *Chemical Reviews*, *119*(24), 12279–12336. https://doi.org/10.1021/acs.chemrev.9b00416

Rice, J. J., May, B. J., Spirou, G. A., & Young, E. D. (1992). Pinna-based spectral cues for sound localization in cat. *Hearing Research*, *58*(2), 132–152. https://doi.org/10.1016/0378-5955(92)90123-5

Schillebeeckx, F., De Mey, F., Vanderelst, D., & Peremans, H. (2011). Biomimetic Sonar: Binaural 3D Localization using Artificial Bat Pinnae. *The International Journal of Robotics Research*, *30*(8), 975–987. https://doi.org/10.1177/0278364910380474

Serafin, S., Geronazzo, M., Erkut, C., Nilsson, N. C., & Nordahl, R. (2018). Sonic Interactions in Virtual Reality: State of the Art, Current Challenges, and Future Directions. *IEEE Computer Graphics and Applications*, *38*(2), 31–43. https://doi.org/10.1109/MCG.2018.193142628

Shao, Y., Zhao, H.-P., Feng, X.-Q., & Gao, H. (2012). Discontinuous crack-bridging model for fracture toughness analysis of nacre. *Journal of the Mechanics and Physics of Solids*, *60*(8), 1400–1419. https://doi.org/10.1016/j.jmps.2012.04.011

Sundar, P. S., Chowdhury, C., & Kamarthi, S. (2021). Evaluation of Human Ear Anatomy and Functionality by Axiomatic Design. *Biomimetics*, *6*(2), 31. https://doi.org/10.3390/biomimetics6020031

Sutlive, J., Singh, A., Zhang, S., & Müller, R. (2020). A biomimetic soft robotic pinna for emulating dynamic reception behavior of horseshoe bats. *Bioinspiration & Biomimetics*, *16*(1), 016016. https://doi.org/10.1088/1748-3190/abbc73

Teshima, Y., Nomura, T., Kato, M., Tsuchiya, T., Shimizu, G., & Hiryu, S. (2022). Effect of bat pinna on sensing using acoustic finite difference time domain simulation. *The Journal of the Acoustical Society of America*, *151*(6), 4039–4045. https://doi.org/10.1121/10.0011737

Wang, Z., Tan, S., Zhang, L., Ren, Y., Wang, Z., & Yang, J. (2021). EarDynamic. *Proceedings of the ACM on Interactive, Mobile, Wearable and Ubiquitous Technologies*, *5*(1), 1–27. https://doi.org/10.1145/3448098

Xu, Y., Afshar, S., Wang, R., Cohen, G., Singh Thakur, C., Hamilton, T. J., & van Schaik, A. (2021). A Biologically Inspired Sound Localisation System Using a Silicon Cochlea Pair. *Applied Sciences*, *11*(4), 1519. https://doi.org/10.3390/app11041519

Yin, X., & Müller, R. (2021). Integration of deep learning and soft robotics for a biomimetic approach to nonlinear sensing. *Nature Machine Intelligence*, *3*(6), 507–512. https://doi.org/10.1038/s42256-021-00330-1

ZALAPA, S. S., Guerrero-Vázquez, S., Sánchez-Hernández, C., Morales-Malacara, J. B., Castaño-Meneses, G., Navarrete-Heredia, J. L., ... & PADILLA-RAMÍREZ, F. J. (2022). Necrotic lesions and associated mites of the pinnae of free-living bats Artibeus jamaicensis and Sturnira hondurensis from Mexico. *Western North American Naturalist*, *82*(4), 760-765.

Zhang, L., & Mueller, R. (2022). Large-scale recognition of natural landmarks with deep learning based on biomimetic sonar echoes. *Bioinspiration & Biomimetics*. https://doi.org/10.1088/1748-3190/ac4c94

99 Micro Servo. (n.d.). *Reefs RC*. https://reefsrc.com/products/99-micro-servo

Appendix

The appendix comprises 13 sections, including the Design Space Code, implemented in MATLAB to generate random configurations for distributing actuators across the pinna. The Program Test section outlines the parameters utilized in the Design Space. Additionally, there is PCA code in MATLAB to compute eigenvalues, as well as GA (Genetic Algorithm) code for optimization. Specifications for alternative servos are included for comparison with the selected servo. Eigenvalue results are provided for both parallel and nonparallel configurations, along with a parametric study for both scenarios. The results for each node in parallel and nonparallel setups are detailed. Furthermore, a parametric study for optimization is conducted, and the corresponding results for each node are presented. For comprehensive details, please refer to the link below.

https://figshare.com/s/de04f02396c3c232d14a